

## Highlights

**Location and Scale-Invariant Power Transformations for Transforming Data to Normality**

Alex Zwanenburg, Steffen Löck

- Research highlight 1
- Research highlight 2

# Location and Scale-Invariant Power Transformations for Transforming Data to Normality

Alex Zwanenburg<sup>a,b,\*</sup>, Steffen Löck<sup>b,c,d</sup>

<sup>a</sup> National Center for Tumor Diseases Dresden (NCT/UCC): German Cancer Research Center (DKFZ), Heidelberg, Germany; Faculty of Medicine and University Hospital Carl Gustav Carus, TUD Dresden University of Technology, Dresden, Germany; Helmholtz-Zentrum Dresden-Rossendorf (HZDR), Dresden, Germany, Fetscherstraße 74/PF 64, Dresden, 01307, Germany

<sup>b</sup> OncoRay – National Center for Radiation Research in Oncology, Faculty of Medicine and University Hospital Carl Gustav Carus, TUD Dresden University of Technology, Helmholtz-Zentrum Dresden-Rossendorf, Fetscherstraße 74/PF 41, Dresden, 01307, Germany

<sup>c</sup> Department of Radiotherapy and Radiation Oncology, Faculty of Medicine and University Hospital Carl Gustav Carus, TUD Dresden University of Technology, Fetscherstraße 74/PF 50, Dresden, 01307, Germany

<sup>d</sup> German Cancer Consortium (DKTK), Partner Site Dresden, and German Cancer Research Center (DKFZ), Im Neuenheimer Feld 280, Heidelberg, 69192, Germany

---

## Abstract

*Keywords:*

---

## 1. Introduction

Many statistical and some machine learning methods assume normality of the underlying data, e.g. analysis of variance and linear discriminant analysis. However, numerical features in datasets may strongly deviate from normal distributions, e.g. by being skewed. Power transformations aim to stabilise variance and improve normality of such features (Bartlett 1947; John W. Tukey 1957). The two most commonly used transformations are that of Box and Cox (1964) and Yeo and Johnson (2000). The Box-Cox transformation of a feature value  $x_i$  of feature  $\mathbf{X} = \{x_1, x_2, \dots, x_n\}$  under the transformation parameter  $\lambda$  is defined as:

---

\*corresponding author

Email address: alexander.zwanenburg@nct-dresden.de (Alex Zwanenburg)

$$\phi_{\text{BC}}^\lambda(x_i) = \begin{cases} (x_i^\lambda - 1) / \lambda & \text{if } \lambda \neq 0 \\ \log(x_i) & \text{if } \lambda = 0 \end{cases} \quad (1)$$

One limitation of the Box-Cox transformation is that it is only defined for  $x_i > 0$ . In contrast, the Yeo-Johnson transformation under the transformation parameter  $\lambda$  is defined for any  $x_i \in \mathbb{R}$ :

$$\phi_{\text{YJ}}^\lambda(x_i) = \begin{cases} ((1 + x_i)^\lambda - 1) / \lambda & \text{if } \lambda \neq 0 \text{ and } x_i \geq 0 \\ \log(1 + x_i) & \text{if } \lambda = 0 \text{ and } x_i \geq 0 \\ -((1 - x_i)^{2-\lambda} - 1) / (2 - \lambda) & \text{if } \lambda \neq 2 \text{ and } x_i < 0 \\ -\log(1 - x_i) & \text{if } \lambda = 2 \text{ and } x_i < 0 \end{cases} \quad (2)$$

The  $\lambda$ -parameter is typically optimised using maximum likelihood estimation under the assumption that the transformed feature is normally distributed. As noted by Raymaekers and Rousseeuw, this approach is sensitive to outliers, and robust versions of Box-Cox and Yeo-Johnson transformations were devised (Raymaekers and Rousseeuw 2024).

Applying a power transformation does not guarantee that transformed features are normally distributed. Depending on location and scale of a feature and the presence of outliers, power transformations may decrease normality, as shown in Figure 1. If normality of the transformed feature is not checked, e.g. in automated power transformation in machine learning workflows, several issues may arise. For example, statistical tests such as ANOVA may produce incorrect results due to violation of the normality assumption. Likewise, machine learning methods that assume normality of input features may suffer a decrease in performance. Moreover, large negative or positive  $\lambda$ -parameters may lead to numeric issues in any subsequent computations.

Statistical tests for normality, such as the Shapiro-Wilk test (Shapiro and Wilk 1965), could be automatically applied to transformed features. However, given sufficiently large sample sizes such tests can detect trivial deviations from normality, and may lead to rejection of sufficiently good power transformations.

To address these issues, we make the following contributions:

- We devise location- and scale-invariant versions of the Box-Cox and Yeo-Johnson transformation, including versions robust to outliers.

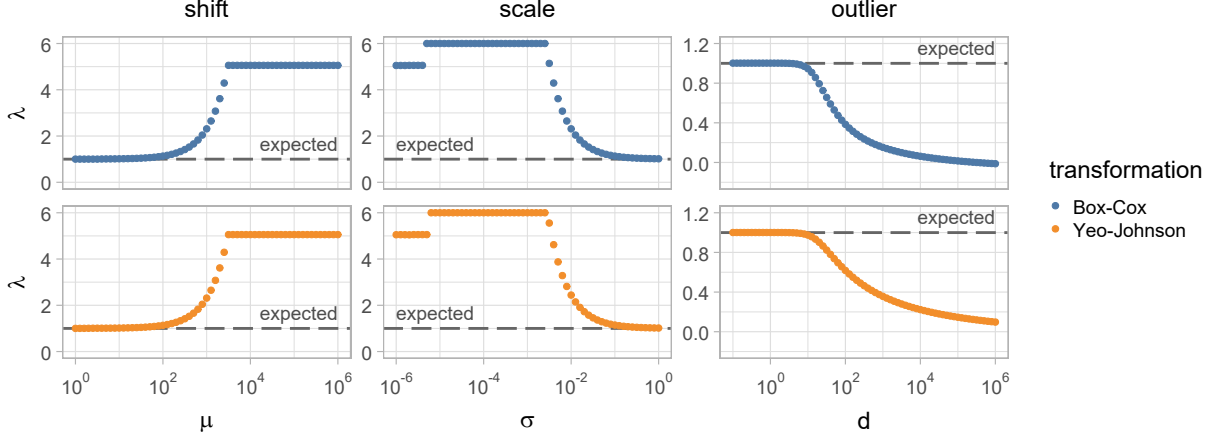


Figure 1: Effect of location, scale and outliers on estimation of the Box-Cox and Yeo-Johnson transformation parameter  $\lambda$ . 10000 samples were drawn from a normal distribution:  $\mathcal{N}(\mu, 1)$  for the shift dataset,  $\mathcal{N}(10, \sigma)$  for the scale dataset and  $\mathcal{N}(0, 1)$  for the outlier dataset. Additionally, an outlier with value  $d$  was added to the outlier dataset. Since samples are drawn from a normal distribution, a transformation parameter of  $\lambda = 1$  is expected. However, a large shift in location, a scale that is small compared to the location, or presence of large outliers lead to incorrectly estimated transformation parameter values.

- We derive the maximum likelihood criterion for location- and scale-invariant Box-Cox and Yeo-Johnson transformations to allow for optimising transformation parameters.
- We define an empirical central normality test for detecting cases where power transformations fail to yield an approximately normally distributed transformed feature.
- We assess the effect of power transformations on the performance of machine learning models.

## 2. Theory

In this section, we will first introduce location- and scale-invariant versions of the Box-Cox and Yeo-Johnson transformations. Subsequently, we define weighted location- and scale-invariant transformations and weighting methods for robust transformations. We then define the quantile function for asymmetric generalised normal distributions to enable random sampling.

Finally, we define the overall framework for the empirical central normality test.

### 2.1. Location- and scale-invariant power transformation

Box-Cox and Yeo-Johnson transformations are modified by introducing shift parameter  $x_0$  and scale parameter  $s$  into equations 1 and 2. The location- and scale-invariant Box-Cox transformation of a feature value  $x_i$  of feature  $\mathbf{X}$  under transformation parameter  $\lambda$ , shift parameter  $x_0$  and scale parameter  $s$  is then:

$$\phi_{BC}^{\lambda,x_0,s}(x_i) = \begin{cases} \left( \left( \frac{x_i - x_0}{s} \right)^\lambda - 1 \right) / \lambda & \text{if } \lambda \neq 0 \\ \log \left[ \frac{x_i - x_0}{s} \right] & \text{if } \lambda = 0 \end{cases} \quad (3)$$

where  $x_i - x_0 > 0$ . Likewise, the location- and scale-invariant Yeo-Johnson transformation of a feature value  $x_i$  under transformation parameter  $\lambda$ , shift parameter  $x_0$  and scale parameter  $s$  is:

$$\phi_{YJ}^{\lambda,x_0,s}(x_i) = \begin{cases} \left( \left( 1 + \frac{x_i - x_0}{s} \right)^\lambda - 1 \right) / \lambda & \text{if } \lambda \neq 0 \text{ and } x_i - x_0 \geq 0 \\ \log \left[ 1 + \frac{x_i - x_0}{s} \right] & \text{if } \lambda = 0 \text{ and } x_i - x_0 \geq 0 \\ - \left( \left( 1 - \frac{x_i - x_0}{s} \right)^{2-\lambda} - 1 \right) / (2 - \lambda) & \text{if } \lambda \neq 2 \text{ and } x_i - x_0 < 0 \\ - \log \left[ 1 - \frac{x_i - x_0}{s} \right] & \text{if } \lambda = 2 \text{ and } x_i - x_0 < 0 \end{cases} \quad (4)$$

For both invariant transformations,  $\lambda$ ,  $x_0$  and  $s$  parameters can be obtained by maximising the log-likelihood function, i.e. using maximum likelihood estimation (MLE). A full derivation of the log-likelihood function for both transformations is shown in Appendix A. The location- and scale-invariant Box-Cox log-likelihood function is:

$$\begin{aligned} \hat{\psi}_{BC}^{\lambda,x_0,s} = & -\frac{n}{2} \log [2\pi\sigma^2] - \frac{1}{2\sigma^2} \sum_{i=1}^n \left( \phi_{BC}^{\lambda,x_0,s}(x_i) - \mu \right)^2 \\ & - n\lambda \log s + (\lambda - 1) \sum_{i=1}^n \log [x_i - x_0] \end{aligned} \quad (5)$$

subject to  $x_i - x_0 > 0$ .  $\mu$  and  $\sigma^2$  are the mean and variance of the Box-Cox transformed feature  $\phi_{BC}^{\lambda,x_0,s}(\mathbf{X})$ , respectively. Similarly, the location- and scale-invariant Yeo-Johnson log-likelihood function is:

$$\hat{\psi}_{YJ}^{\lambda, x_0, s} = -\frac{n}{2} \log [2\pi\sigma^2] - \frac{1}{2\sigma^2} \sum_{i=1}^n \left( \phi_{YJ}^{\lambda, x_0, s}(x_i) - \mu \right)^2 \\ - n \log s + (\lambda - 1) \sum_{i=1}^n \text{sgn}(x_i - x_0) \log \left[ 1 + \frac{|x_i - x_0|}{s} \right] \quad (6)$$

where  $\mu$  and  $\sigma^2$  are the mean and variance of the Yeo-Johnson transformed feature  $\phi_{YJ}^{\lambda, x_0, s}(\mathbf{X})$ , respectively.

## 2.2. Robust location- and scale-invariant power transformations

Real-world data may contain outliers, to which maximum likelihood estimation can be sensitive. Their presence may lead to poor transformations to normality, as shown in Figure 1. As indicated by Raymaekers and Rousseeuw (2024), the general aim of power transformations should be to transform non-outlier data to normality, i.e. achieve *central normality*. To achieve this, they devised an iterative procedure to find a robust estimate of the transformation parameter  $\lambda$ . Briefly, this process requires identifying outliers in the data and weighting such instances during the optimisation process. Raymaekers and Rousseeuw (2024) achieve this through weighted maximum likelihood estimation. However, because this procedure iteratively estimates and updates  $\lambda$ , it can not be used here to simultaneously estimate  $\lambda$ ,  $x_0$  and  $s$  for location- and scale-invariant power transformations. Nonetheless, as a procedure, weighted MLE can be used for estimating the transformation, shift and scale parameters.

Here, weighted maximum likelihood estimation is based on equations 5 and 6. Compared to Raymaekers and Rousseeuw (2024), these log-likelihood functions includes additional terms to accommodate estimation of  $x_0$  and  $s$ . The weighted location- and scale-invariant Box-Cox log-likelihood function is:

$$\hat{\psi}_{rBC}^{\lambda, x_0, s} = -\frac{1}{2} \left( \sum_{i=1}^n w_i \right) \log [2\pi\sigma_w^2] - \frac{1}{2\sigma_w^2} \sum_{i=1}^n w_i \left( \phi_{BC}^{\lambda, x_0, s}(x_i) - \mu_w \right)^2 \\ - \lambda \left( \sum_{i=1}^n w_i \right) \log s + (\lambda - 1) \sum_{i=1}^n w_i \log [x_i - x_0] \quad (7)$$

where  $\mu_w$  and  $\sigma_w^2$  are the weighted mean and weighted variance of the Box-Cox transformed feature  $\phi_{\text{BC}}^{\lambda,x_0,s}(\mathbf{X})$ :

$$\sigma_w^2 = \frac{\sum_{i=1}^n w_i (\phi_{\text{BC}}^{\lambda,x_0,s}(x_i) - \mu_w)^2}{\sum_{i=1}^n w_i} \quad \text{with } \mu_w = \frac{\sum_{i=1}^n w_i \phi_{\text{BC}}^{\lambda,x_0,s}(x_i)}{\sum_{i=1}^n w_i} \quad (8)$$

Analogously, the weighted location- and scale-invariant Yeo-Johnson log-likelihood function is:

$$\begin{aligned} \hat{\psi}_{\text{rYJ}}^{\lambda,x_0,s} = & -\frac{1}{2} \left( \sum_{i=1}^n w_i \right) \log [2\pi\sigma_w^2] - \frac{1}{2\sigma_w^2} \sum_{i=1}^n w_i (\phi_{\text{YJ}}^{\lambda,x_0,s}(x_i) - \mu_w)^2 \\ & - \left( \sum_{i=1}^n w_i \right) \log s + (\lambda - 1) \sum_{i=1}^n w_i \text{sgn}(x_i - x_0) \log \left[ 1 + \frac{|x_i - x_0|}{s} \right] \end{aligned} \quad (9)$$

where  $\mu_w$  and  $\sigma_w^2$  are the weighted mean and weighted variance of the Yeo-Johnson transformed feature  $\phi_{\text{YJ}}^{\lambda,x_0,s}(\mathbf{X})$ :

$$\sigma_w^2 = \frac{\sum_{i=1}^n w_i (\phi_{\text{YJ}}^{\lambda,x_0,s}(x_i) - \mu_w)^2}{\sum_{i=1}^n w_i} \quad \text{with } \mu_w = \frac{\sum_{i=1}^n w_i \phi_{\text{YJ}}^{\lambda,x_0,s}(x_i)}{\sum_{i=1}^n w_i} \quad (10)$$

The weights  $w_i$  in equations 7 and 9 can be set using several weighting functions. Using  $x_i$  as an argument that will be defined later, we investigate three weighting functions:

- A step function, with  $\delta_1 \geq 0$  as threshold parameter:

$$w_i = \begin{cases} 1 & \text{if } |x_i| \leq \delta_1 \\ 0 & \text{if } |x_i| > \delta_1 \end{cases} \quad (11)$$

- A triangle function (or generalised Huber weight), with  $\delta_1 \geq 0$  and  $\delta_2 \geq \delta_1$  as threshold parameters:

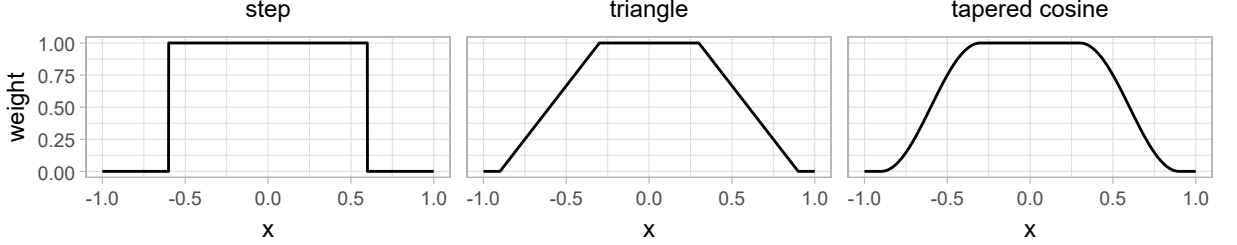


Figure 2: Weighting functions investigated in this study to make power transformations more robust against outliers. In this example, the step function was parameterised with  $\delta_1 = 0.60$ . The triangle and tapered cosine functions were both parameterised with  $\delta_1 = 0.30$  and  $\delta_2 = 0.90$ .

$$w_i = \begin{cases} 1 & \text{if } |\dot{x}_i| < \delta_1 \\ 1 - \frac{|\dot{x}_i| - \delta_1}{\delta_2 - \delta_1} & \text{if } \delta_1 \leq |\dot{x}_i| \leq \delta_2 \\ 0 & \text{if } |\dot{x}_i| > \delta_2 \end{cases} \quad (12)$$

- A tapered cosine function (J. W. Tukey 1967), with  $\delta_1 \geq 0$  and  $\delta_2 \geq \delta_1$  as threshold parameters:

$$w_i = \begin{cases} 1 & \text{if } |\dot{x}_i| < \delta_1 \\ 0.5 + 0.5 \cos \left( \pi \frac{|\dot{x}_i| - \delta_1}{\delta_2 - \delta_1} \right) & \text{if } \delta_1 \leq |\dot{x}_i| \leq \delta_2 \\ 0 & \text{if } |\dot{x}_i| > \delta_2 \end{cases} \quad (13)$$

All weighting functions share the characteristic that for  $|\dot{x}_i| < \delta_1$ , instances are fully weighted, i.e. when  $\delta_1 > 0$  the weighting functions are symmetric window functions with a flat top. The triangle and tapered cosine functions then gradually down-weight instances with  $\delta_1 \leq |\dot{x}_i| \leq \delta_2$ , and assign no weight to instances  $|\dot{x}_i| > \delta_2$ . Examples of these weighting function are shown in Figure 2.

Each weighting function has an argument  $\dot{x}$  that is related to the (transformed) feature in one of several ways:

- The weighting function uses empirical probabilities of the distribution of the original feature  $\mathbf{X}$ . After sorting  $\mathbf{X}$  in ascending order, probabilities are determined as  $p_i = \frac{i-1/3}{n+1/3}$ , with  $i = 1, 2, \dots, n$ , with  $n$  the number of instances of feature  $\mathbf{X}$ . Then  $\dot{x}_i = p_i^* = 2(p_i - 0.5)$ , so that argument is zero-centered.

- The weighting function uses the z-score of the transformed feature  $\phi^{\lambda, x_0, s}(\mathbf{X})$ . After Raymaekers and Rousseeuw (2024),  $z_i = \frac{\phi^{\lambda, x_0, s}(x_i) - \mu_M}{\sigma_M}$ . Here,  $\mu_M$  and  $\sigma_M$  are robust Huber M-estimates of location and scale of the transformed feature  $\phi^{\lambda, x_0, s}(\mathbf{X})$  (Huber 1981). Then  $\dot{x}_i = z_i$ .
- After sorting  $\mathbf{X}$  in ascending order, the weighting function uses the residual error between the z-score of the transformed feature  $\phi^{\lambda, x_0, s}(\mathbf{X})$  and the theoretical z-score from a standard normal distribution:  $r_i = |(\phi^{\lambda, x_0, s}(x_i) - \mu_M) / \sigma_M - F_N^{-1}(p_i)|$ , with  $\mu_M$ ,  $\sigma_M$  and  $p_i$  as defined above. Then  $\dot{x}_i = r_i$ .

### 2.3. Asymmetric generalised normal distributions

Modifications intended to make power transformations invariant to location and scale of a feature and methods to improve their robustness against outliers need to be assessed using data drawn from a range of different distributions. Since the power transformations are intended for use with unimodal distributions, the generalised normal distribution (Subbotin 1923; Nadarajah 2005) is a suitable option for simulating realistic feature distributions. This distribution has the following probability density function  $f_\beta$  for a value  $x \in \mathbb{R}$ :

$$f_\beta(x) = \frac{\beta}{2\Gamma(1/\beta)} e^{-|x|^\beta} \quad (14)$$

Here,  $\Gamma$  is the gamma function, and  $\beta$  is a strictly positive shape parameter. For  $\beta = 1$ , the probability density function describes a Laplace distribution. A normal distribution is found for  $\beta = 2$ , and for large  $\beta$ , the distribution approaches a uniform distribution. We will refrain from introducing scale and location parameters here directly.

Realistic feature distributions may be skewed. Gijbels et al. describe a recipe for introducing skewness into the otherwise symmetric generalised normal distribution (Gijbels, Karim, and Verhasselt 2019), leading to the following probability density function:

$$f_\alpha(x; \mu, \sigma, \beta) = \frac{2\alpha(1-\alpha)}{\sigma} \begin{cases} f_\beta\left((1-\alpha)\frac{|x-\mu|}{\sigma}\right) & , x \leq \mu \\ f_\beta\left(\alpha\frac{|x-\mu|}{\sigma}\right) & , x > \mu \end{cases} \quad (15)$$

Here,  $\alpha \in (0, 1)$  is a skewness parameter.  $\alpha > 0.5$  creates a distribution with a negative skew, i.e. a left-skewed distribution. A right-skewed distribution is created for  $\alpha < 0.5$ .  $\mu \in \mathcal{R}$  and  $\sigma \in (0, \infty)$  are location and scale

parameters, respectively.  $f_\alpha$  thus describes the probability density function of an asymmetric generalised normal distribution, which we will refer to here and parametrise as  $\mathcal{AGN}(\mu, \sigma, \alpha, \beta)$ .

We require a quantile function (or an approximation thereof) to draw random values from an asymmetric generalised normal distribution using inverse transform sampling. Gijbels et al. derived the following quantile function  $F_\alpha^{-1}(p)$ :

$$F_\alpha^{-1}(p; \mu, \sigma, \beta) = \begin{cases} \mu + \frac{\sigma}{1-\alpha} F_\beta^{-1}\left(\frac{p}{2\alpha}\right) & , p \leq \alpha \\ \mu + \frac{\sigma}{\alpha} F_\beta^{-1}\left(\frac{1+p-2\alpha}{2(1-\alpha)}\right) & , p > \alpha \end{cases} \quad (16)$$

The quantile function for the asymmetric generalised normal distribution  $F_\alpha^{-1}$  thus incorporates the quantile function  $F_\beta^{-1}$  of the symmetric generalised normal distribution.  $F_\beta^{-1}$  was derived by Griffin to be (Griffin 2018):

$$F_\beta^{-1}(p) = \text{sgn}(p - 0.5) F_\Gamma^{-1}(2|p - 0.5|; 1/\beta) \quad (17)$$

Here,  $F_\Gamma^{-1}$  is the quantile function of the gamma distribution with shape  $1/\beta$ , which can be numerically approximated.

#### 2.4. Empirical central normality test

Power transformations aim to transform features to a normal distribution. However, this may not always be successful or possible. Deviations from normality can be detected by normality tests, such as the Shapiro-Wilk test (Shapiro and Wilk 1965). In practice, normality tests may be too stringent with large sample sizes, outliers, or both. Here we develop an empirical test for central normality. The null hypothesis  $H_0$  is that the distribution is centrally normal. The alternative hypothesis  $H_1$  is that the distribution is not centrally normal.

Let central normality be defined as the normality of central portion  $\kappa$  of the data, i.e.  $\mathbf{X}_{\text{central}} = \{x_i \in \mathbf{X} \mid \frac{1-\kappa}{2} \leq p_i \leq \frac{1+\kappa}{2}\}$ , with  $p_i$  probabilities of the empirical distribution, as previously. We then compute the residual errors between the z-scores of the transformed feature  $\phi^{\lambda, x_0, s}(\mathbf{X})$  and the expected z-scores from a standard normal distribution:  $r_i = |(\phi^{\lambda, x_0, s}(x_i) - \mu_M)/\sigma_M - F_{\mathcal{N}}^{-1}(p_i)|$ , with  $\mu_M$  and  $\sigma_M$  robust Huber M-estimates of location and scale of the transformed feature  $\phi^{\lambda, x_0, s}(\mathbf{X})$  (Huber 1981). The set of residual errors for the central portion of the data is then  $\mathbf{R}_{\text{central}} = \{r_i \in \{r_1, r_2, \dots, r_n\} \mid \frac{1-\kappa}{2} \leq p_i \leq \frac{1+\kappa}{2}\}$ .

The test statistic  $\tau_{\text{ecn}}$  is then defined as:

$$\tau_{\text{ecn}} = \frac{\sum_{i=1}^N r_i [r_i \in \mathbf{R}_{\text{central}}]}{\sum_{i=1}^N [r_i \in \mathbf{R}_{\text{central}}]} \quad (18)$$

Here  $[ \cdot ]$  denotes an Iverson bracket. The test statistic is equal to the mean of the residual errors of the central portion of the data.

To use the test statistic, the central portion of the data needs to be defined and the Type 1 error rates determined. We will do so in section 3.

### 3. Simulation

We used simulated data to assess invariance to location and scale of the proposed power transformations, weighting for robust transformations, and to develop the empirical central normality test. The  $\lambda$  parameter for conventional power transformations (Eqn. 1 and 2), as well as  $\lambda$ ,  $x_0$  and  $s$  parameters for location- and scale-invariant power transformations (Eqn. 3 and 4) were estimated using the BOBYQA algorithm for derivative-free bound constraint optimisation (Powell 2009) through maximum likelihood estimation. The required algorithms were implemented in the `power.transform` R software package (Zwanenburg and Löck 2024b) (version 1.0.0). Of note, the `power.transform` package shifts feature values into the positive domain if negative or zero values are present for Box-Cox power transformations.

#### 3.1. Invariance to location and scale

To assess whether the proposed power transformations lead to values of  $\lambda$  that are invariant to location and scale of the distribution, we simulated three different distributions. We first randomly drew 10000 values from a normal distribution:  $\mathbf{X}_{\text{normal}} = \{x_1, x_2, \dots, x_{10000}\} \sim \mathcal{N}(0, 1)$ , or equivalently  $\mathbf{X}_{\text{normal}} = \{x_1, x_2, \dots, x_{10000}\} \sim \mathcal{AGN}(0, 1/\sqrt{2}, 0.5, 2)$ . The second distribution was a right-skewed generalised normal distribution  $\mathbf{X}_{\text{right}} = \{x_1, x_2, \dots, x_{10000}\} \sim \mathcal{AGN}(0, 1/\sqrt{2}, 0.2, 2)$ . The third distribution was a left-skewed generalised normal distribution  $\mathbf{X}_{\text{left}} = \{x_1, x_2, \dots, x_{10000}\} \sim \mathcal{AGN}(0, 1/\sqrt{2}, 0.8, 2)$ . We then computed transformation parameter  $\lambda$  using the original definitions (Eqn. 1 and 2) and the location- and scale-invariant definitions (Eqn. 3 and 4) for each distribution. To assess location invariance, a positive value  $d_{\text{shift}}$  was added to each distribution with  $d_{\text{shift}} \in [1, 10^6]$ . Similarly, to assess scale invariance, each distribution was multiplied by a positive value  $d_{\text{scale}}$ , where  $d_{\text{scale}} \in [1, 10^6]$ .

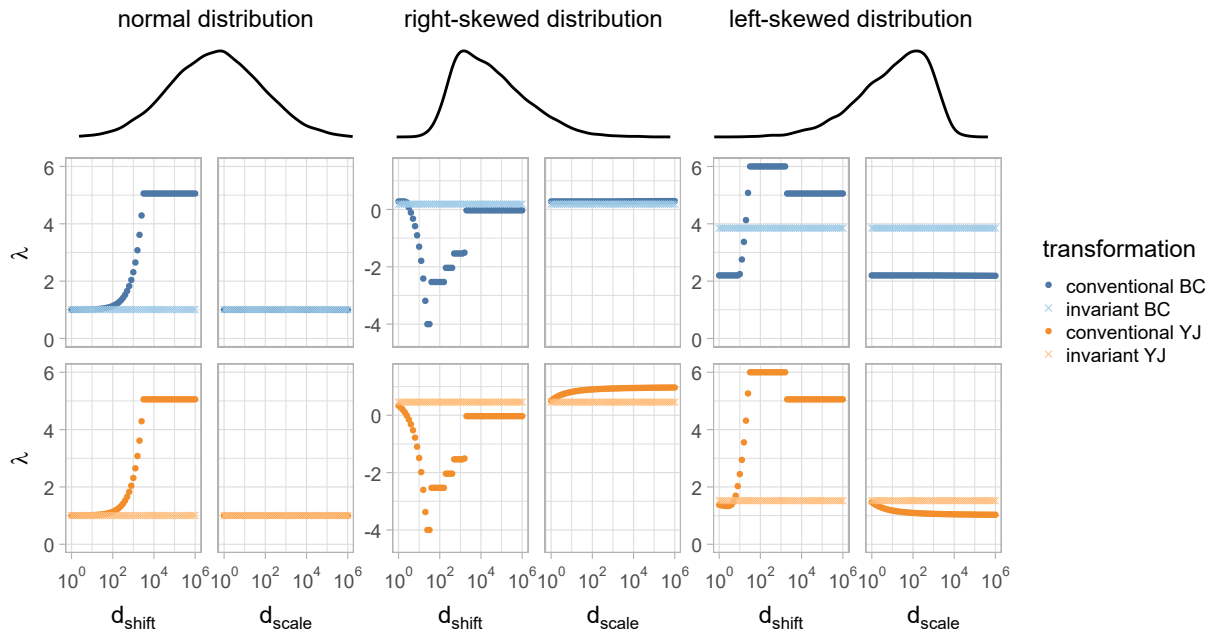


Figure 3: Invariant power transformation produces transformation parameters that are invariant to location and scale. Samples were drawn from normal, right-skewed and left-skewed distributions, respectively, which then underwent a shift  $d_{\text{shift}}$  or multiplication by  $d_{\text{scale}}$ . Estimates of the transformation parameter  $\lambda$  for the conventional power transformations show strong dependency on the overall location and scale of the distribution, whereas estimates obtained for the location- and scale-invariant power transformations are constant.

The result is shown in Figure 3. For each distribution, transformation parameter  $\lambda$  varied with  $d_{\text{shift}}$  and  $d_{\text{scale}}$  when estimated for conventional transformations. In contrast, estimation of  $\lambda$  for invariant power transformations was invariant to both  $d_{\text{shift}}$  and  $d_{\text{scale}}$ .

### 3.2. Robust transformations

Outliers may be present in data and affect estimation of transformation parameters. The log-likelihood function can be weighted to assign less weight to outlier instances, see equations 7 and 9. We proposed three weighting function: step, triangle and tapered cosine, that have one, two and two parameters, respectively. Each weighting function then takes one of three values as input: probabilities of the empirical distribution of the original feature, the z-score of the transformed feature values, or the residual error between the z-score of the transformed feature values and their expected z-score based on the normal distribution.

To determine the weighting function parameters for each of the nine combinations,  $m_d = 100$  asymmetric generalised normal distributions were drawn. Each distribution was parametrised with a randomly chosen skewness parameter  $\alpha \sim U(0.01, 0.99)$  and shape parameter  $\beta \sim U(1.00, 5.00)$ . Location and scale parameters were set as  $\mu = 0$  and  $\sigma = 1$ , respectively.  $n = \lceil 10^7 \rceil$  instances were then randomly drawn, with  $\gamma \sim U(2, 4)$ , i.e., between 100 and 10000 values are drawn to create  $\mathbf{X}_i$ .

Outlier values were then drawn to randomly replace a fraction of the values of  $\mathbf{X}_i$ . This was repeated  $m_{\text{out}} = 10$  times, with outlier fractions regularly spaced in  $[0.00, 0.10]$ . Thus up to 10 percent of the values could be replaced by outliers. Outlier values were set according to John W. Tukey (1977), as follows. Let  $x^* \sim U(-2, 2)$ . Then the corresponding outlier value was:

$$x_{\text{out}} = \begin{cases} Q_1 - (1.5 - x^*) \text{IQR} & \text{if } x^* < 0 \\ Q_3 + (1.5 + x^*) \text{IQR} & \text{if } x^* \geq 0 \end{cases} \quad (19)$$

$Q_1$ ,  $Q_3$  and IQR are the first quartile, third quartile and interquartile range of  $\mathbf{X}_i$ , respectively. Outlier values randomly replaced values in  $\mathbf{X}_i$  to create  $\mathbf{X}_{i,j}$ , with  $j \in \{1, \dots, m_{\text{out}}\}$

To find the optimal values for the weighting function parameters  $\delta_1$  and  $\delta_2$  (if applicable), we minimised the absolute difference between the  $\lambda_r$  parameter obtained for robust transformation in the presence of outliers, and

Table 1: Optimal weighting parameters and corresponding loss for location- and scale-invariant Box-Cox power transformations.  $p^*$  indicates use of the empirical distribution of feature values,  $z$  the z-score of the transformed feature values, and  $r$  the residual error between the z-score of transformed feature values and the expected z-score according to the normal distribution. The *initial* column shows the starting parameter value for the optimisation process, with the corresponding boundary values in the *limits* column. The optimal column shows the optimal parameter values. The *loss* column shows the loss achieved by each method, under optimised parameters. Lower loss indicates better robustness against outliers.

method	$\delta_1$			$\delta_2$			loss
	initial	limits	optimal	initial	limits	optimal	
non-robust	—	—	—	—	—	—	771
$p^*$ (step)	0.80	(0, 1]	0.86	—	—	—	561
$p^*$ (triangle)	0.80	(0, 1]	0.83	0.95	(0, 1]	0.92	564
$p^*$ (tapered cosine)	0.80	(0, 1]	0.76	0.95	(0, 1]	0.95	560
$z$ (step)	1.28	(0, 10]	1.12	—	—	—	1153
$z$ (triangle)	1.28	(0, 10]	0.38	1.96	(0, 10]	4.48	1178
$z$ (tapered cosine)	1.28	(0, 10]	1.21	1.96	(0, 10]	4.92	1135
$r$ (step)	0.50	(0, 10]	2.18	—	—	—	1839
$r$ (triangle)	0.50	(0, 10]	1.29	1.00	(0, 10]	1.47	1764
$r$ (tapered cosine)	0.50	(0, 10]	1.38	1.00	(0, 10]	1.41	1583

the  $\lambda_0$  parameter obtained using the non-robust transformations in absence of outliers:

$$\left\{ \hat{\delta}_1, \hat{\delta}_2 \right\} = \underset{\delta_1, \delta_2}{\operatorname{argmin}} \sum_{i=1}^{m_d} \sum_{j=1}^{m_{\text{out}}} |\lambda_r(\mathbf{X}_{i,j}; \delta_1, \delta_2) - \lambda_0(\mathbf{X}_i)| \quad (20)$$

Minimisation was conducted using the BOBYQA algorithm for derivative-free bound constraint optimisation (Powell 2009). The resulting weighting function parameters for weighted MLE are shown in Tables 1 and 2 for robust location- and scale-invariant Box-Cox and Yeo-Johnson transformations, respectively.

Figure 4 shows the distribution of errors  $|\lambda_r - \lambda_0|$  for non-robust and robust transformations using the optimal weighting function parameters. In the presence of outliers, the Yeo-Johnson transformation yielded smaller er-

Table 2: Optimal weighting parameters and corresponding loss for location- and scale-invariant Yeo-Johnson power transformations.  $p^*$  indicates use of the empirical distribution of feature values,  $z$  the z-score of the transformed feature values, and  $r$  the residual error between the z-score of transformed feature values and the expected z-score according to the normal distribution. The *initial* column shows the starting parameter value for the optimisation process, with the corresponding boundary values in the *limits* column. The *optimal* column shows the optimal parameter values. The *loss* column shows the loss achieved by each method, under optimised parameters. Lower loss indicates better robustness against outliers.

method	$\delta_1$			$\delta_2$			loss
	initial	limits	optimal	initial	limits	optimal	
non-robust	—	—	—	—	—	—	364
$p^*$ (step)	0.80	(0, 1]	0.95	—	—	—	224
$p^*$ (triangle)	0.80	(0, 1]	0.88	0.95	(0, 1]	0.97	212
$p^*$ (tapered cosine)	0.80	(0, 1]	0.94	0.95	(0, 1]	0.95	218
$z$ (step)	1.28	(0, 10]	1.09	—	—	—	392
$z$ (triangle)	1.28	(0, 10]	0.24	1.96	(0, 10]	4.62	396
$z$ (tapered cosine)	1.28	(0, 10]	0.15	1.96	(0, 10]	6.05	413
$r$ (step)	0.50	(0, 10]	1.63	—	—	—	746
$r$ (triangle)	0.50	(0, 10]	1.50	1.00	(0, 10]	1.79	731
$r$ (tapered cosine)	0.50	(0, 10]	1.51	1.00	(0, 10]	1.57	612

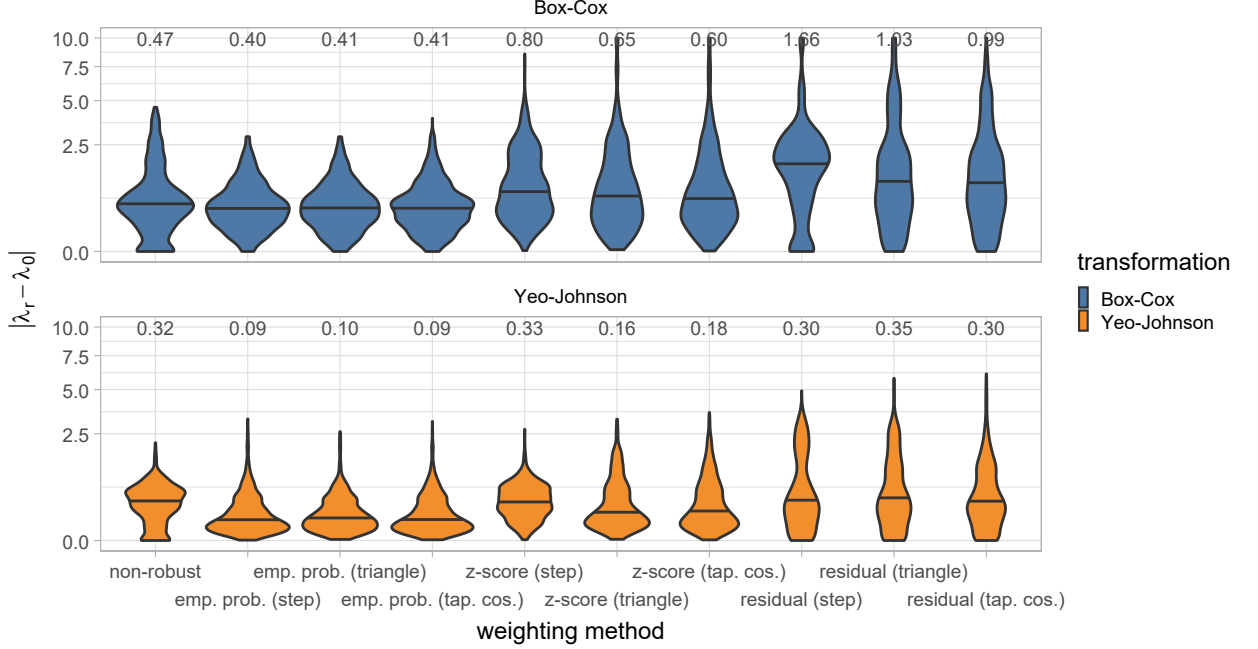


Figure 4: Robustness of power transformations after optimising weighting function parameters. The distribution of errors, i.e. the difference between robustly fitted  $\lambda^r$  and expected  $\lambda_0$  found in the absence of outliers, is shown for 1000 randomly parametrised asymmetric generalised normal distributions with up to 10% outliers on either side of the distribution. The top and bottom panel show errors for the location- and scale-invariant Box-Cox and Yeo-Johnson transformations, respectively. In each panel, the error distribution for the non-robust transformation is shown to the left for comparison with different weighting methods. Note that a square root transformation was applied along the  $y$ -axis for display purposes. Median errors are shown above each distribution.

rors than the Box-Cox transformation. For both transformations, weighting based on empirical probabilities yielded the most consistent  $\lambda$  parameter estimates in the presence of outliers. Other methods did not outperform the non-robust transformation method.

### 3.3. Empirical central normality test

To develop an empirical test for central normality we need to consider two parameters: the central portion  $\kappa$  as a fixed parameter, and test statistic  $\tau_{\text{ecn}}$ . We will first define the central portion  $\kappa$ .

First we draw  $m_d = 10000$  random asymmetric generalised normal distributions. As before, each distribution is parametrised with a randomly

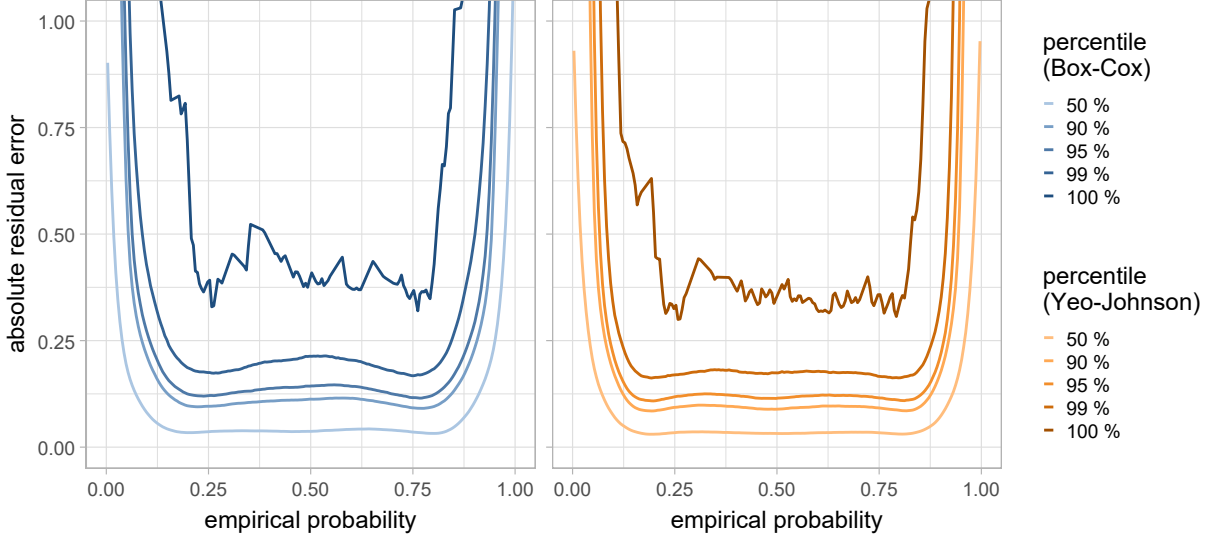


Figure 5: Residual error as a function of empirical probability. Percentiles of the error are shown for robust, location- and scale-invariant transformations of 10000 randomly drawn asymmetric generalised normal distributions, for each of which outliers were randomly drawn 10 times (up to 10% of samples). Larger errors occur at the edges of each distribution.

chosen skewness parameter  $\alpha \sim U(0.01, 0.99)$  and shape parameter  $\beta \sim U(1.00, 5.00)$ . Location and scale parameters are set as  $\mu = 0$  and  $\sigma = 1$ , respectively.  $n = \lceil 10^\gamma \rceil$  values are then randomly drawn, with  $\gamma \sim U(1.47, 3.00)$ , which leads to between 30 and 1000 values being drawn to create  $\mathbf{X}_i$ . As before, for each distribution, up to 10% of instances are replaced by outlier values, and this is repeated 10 times. We then compute residuals after optimising robust location- and scale-invariant transformations with the empirical tapered cosine weighting method.

Figure 5 shows the residual errors of the transformed distribution as function of the empirical probability. As expected, the largest deviations from normality appear on the extremities of this range. For Box-Cox transformations, the effect of outliers on the lower end of the distribution leads to noticeable asymmetry. Between very low and very high empirical probabilities, residual errors are constrained and relatively flat. This is the candidate range for the central portion of the data.

We then consider the empirical probability of type I errors: the probability of incorrectly classifying a centrally normal distribution as being non-

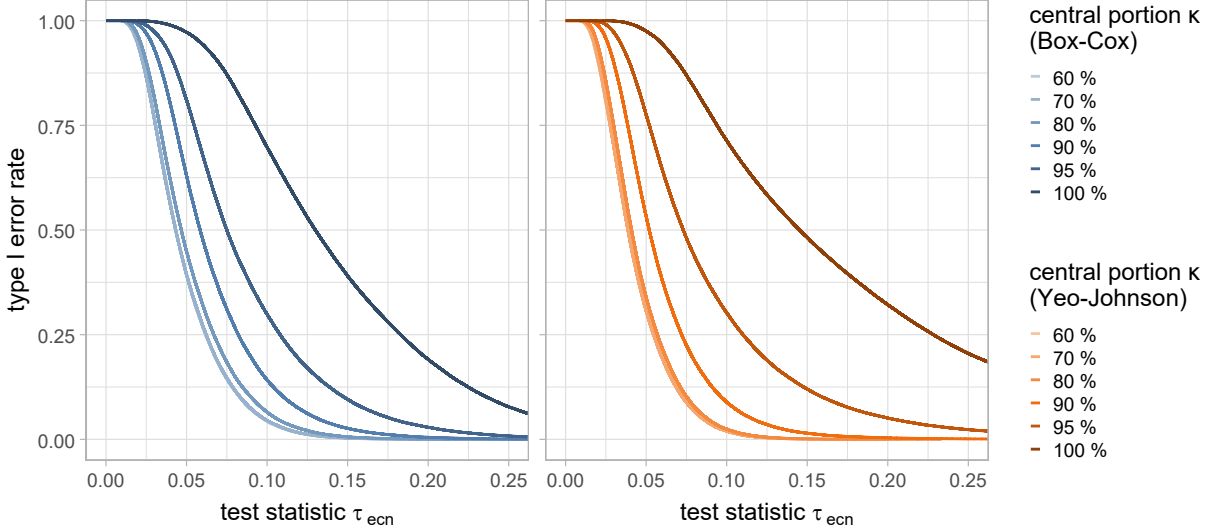


Figure 6: Type 1 error rate of transformed asymmetric generalised normal distributions as function of the test statistic  $\tau_{\text{ecn}}$  for the central portion  $\kappa$  of the distribution.

Table 3: Test statistic  $\tau_{\text{ecn}}$  for empirical central normality at  $\kappa = 0.80$  as a function of Type I error rate.

type I error rate	0.50	0.20	0.10	0.05	0.02	0.01	0.001
$\tau_{\text{ecn}}$	0.041	0.062	0.075	0.088	0.103	0.115	0.154

normal based on the test statistic  $\tau_{\text{ecn}}$ . Under the assumption that the asymmetric generalised normal distributions are centrally normal after robust transformation, this produces the relationship shown in Figure 6. Since for  $\kappa \leq 0.80$  error curves for both transformation methods are similar, we fix the value of the central portion  $\kappa$  to 0.80. In the remaining we will use the empirical central normality test statistic values defined using robust location- and scale-invariant Yeo-Johnson transformations, as it is more conservative (see Appendix E). This leads to test statistic values listed in Table 3

In Figure 7 we apply the empirical central normality test to assess central normality of features that are composed of a mixture of samples drawn from two normal distributions. With increased separation of the underlying normal distributions, the probability of the feature being centrally normal decreases, as expected.

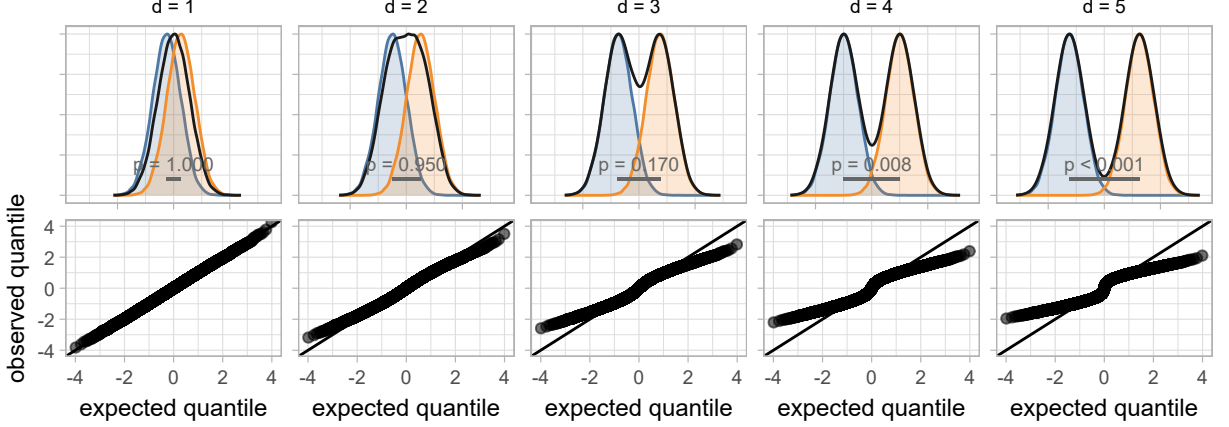


Figure 7: Bi-modal distributions and empirical central normality test results. The feature (black) is a mixture of two identical sample sets (blue and orange) drawn from normal distributions that are offset by a distance  $d$ . We use the empirical centrally normality test to compute the probability for the hypothesis that the distribution is centrally normal. As may be observed, with increasing offset  $d$  the probability that the feature is centrally normal decreases. Quantile-quantile plots are drawn below each distribution.

## 4. Experimental Results

### 4.1. Invariance

Location- and scale-invariant power transformations are intended to yield improved transformations to normality in the presence of large shifts in location, distributions that due to location and scale are not centered near zero, or both. Earlier, we assessed these transformations using simulated data. In the following, they are evaluated using examples from real datasets. We focus on the Yeo-Johnson transformation because of its ability to handle features with negative values. Results for Box-Cox transformations are shown in Appendix D.

#### 4.1.1. Age of patients with lung cancer

A common feature in health-related datasets is age. Here we use data on 228 patients with lung cancer that was collected and published by Loprinzi et al. (Loprinzi et al. 1994). The age in the cohort was  $62.4 \pm 9.1$  (mean  $\pm$  standard deviation) years. Applying conventional and invariant Yeo-Johnson transformations to patient age yielded the following results, see Figure 8: no transformation (sum of residuals with normal distribution  $\sum r_i = 16.5$ ); conventional transformation ( $\lambda = 2.0$ ,  $\sum r_i = 11.5$ ,  $\mu_{YJ} = 1.8 \cdot 10^3$ ,  $\sigma_{YJ} = 0.5$ .

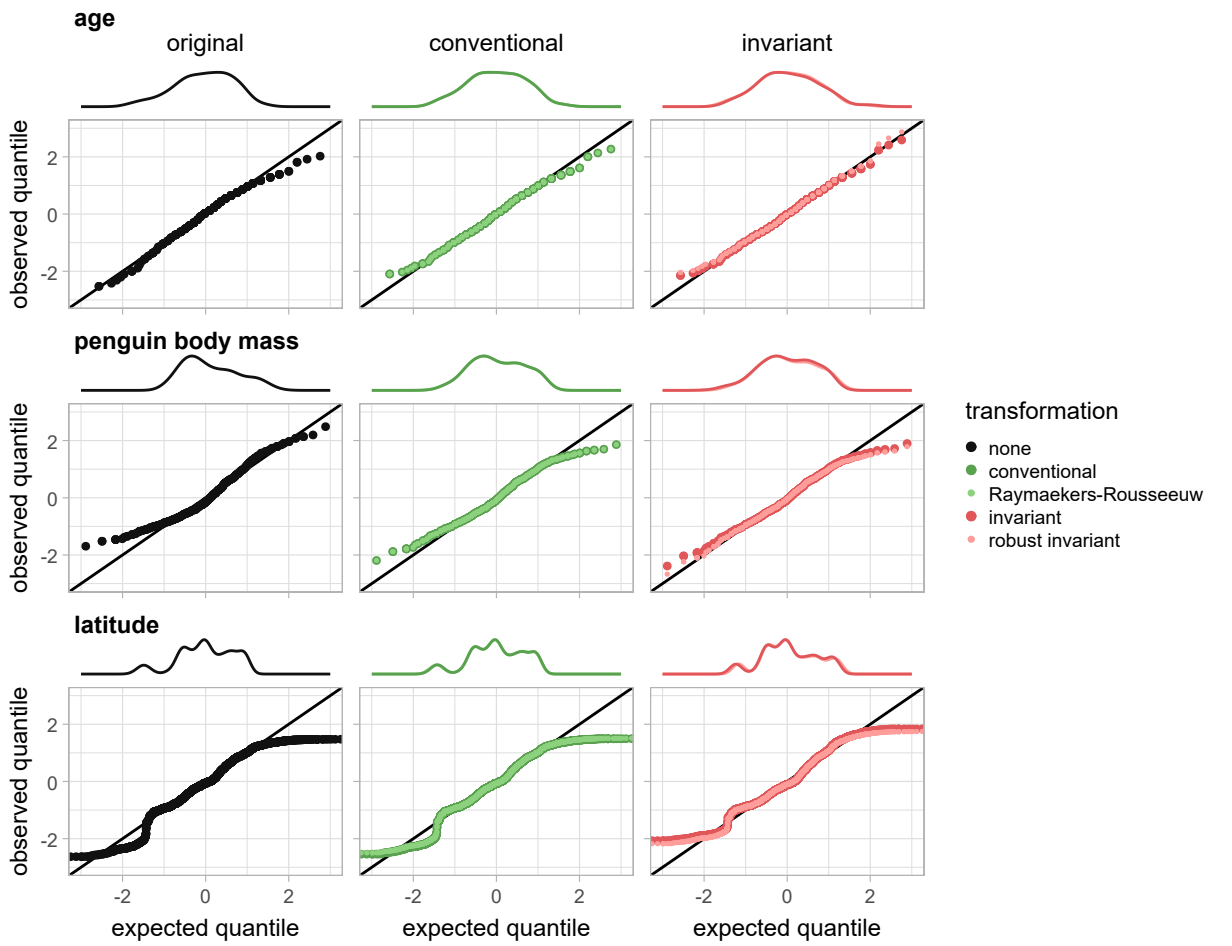


Figure 8: Quantile-quantile plots for several datasets: age of patients with lung cancer (top row); penguin body mass (middle row); and latitude coordinates of houses sold in Ames, Iowa (bottom row). Multiple quantile-quantile plots are shown: for the original feature (left column); the feature transformed using the conventional Yeo-Johnson transformation and Raymaekers and Rousseeuw's robust adaptation (middle column); and the feature transformed using the non-robust and robust location- and scale invariant Yeo-Johnson transformations (right column).

$10^3$ ); Raymaekers and Rousseeuw's robust adaptation ( $\lambda = 2.0$ ,  $\sum r_i = 11.5$ ,  $\mu_{YJ} = 1.8 \cdot 10^3$ ,  $\sigma_{YJ} = 0.5 \cdot 10^3$ ); location- and scale-invariant transformation ( $\lambda = 0.9$ ,  $\sum r_i = 8.8$ ,  $\mu_{YJ} = 1.2$ ,  $\sigma_{YJ} = 1.1$ ); and robust location- and scale-invariant transformation ( $\lambda = 0.8$ ,  $\sum r_i = 10.6$ ,  $\mu_{YJ} = 1.2$ ,  $\sigma_{YJ} = 1.0$ ).

Location- and scale-invariant transformation led to a lower overall residual sum, indicating a better transformation. Robust location- and scale-invariant transformation had a higher residual sum compared to the non-robust variant, which may be due to the lack of outliers in the data. Conventional transformations inflated the mean  $\mu_{YJ}$  and standard deviation  $\sigma_{YJ}$  of the age feature after transformation. The empirical central normality test did not detect any statistically significant deviations from central normality for any transformation (all  $p \geq 0.78$ ).

#### 4.1.2. Penguin body mass

Gorman, Williams and Fraser recorded body mass (in grams) of 342 penguins of three different species (Gorman, Williams, and Fraser 2014). The body mass was  $(4.2 \pm 0.8) \cdot 10^3$  (mean  $\pm$  standard deviation) grams, and not centrally normal ( $p = 0.03$ ). Applying conventional and invariant Yeo-Johnson transformations to body mass yielded the following results, see Figure 8: no transformation (residual sum  $\sum r_i = 48.0$ ); conventional transformation ( $\lambda = -0.5$ ,  $\sum r_i = 32.2$ ,  $\mu_{YJ} = 2.1$ ,  $\sigma_{YJ} = 4 \cdot 10^{-3}$ ); Raymaekers and Rousseeuw's robust adaptation ( $\lambda = -0.5$ ,  $\sum r_i = 32.2$ ,  $\mu_{YJ} = 2.1$ ,  $\sigma_{YJ} = 4 \cdot 10^{-3}$ ); location- and scale-invariant transformation ( $\lambda = 0.5$ ,  $\sum r_i = 26.8$ ,  $\mu_{YJ} = 0.9$ ,  $\sigma_{YJ} = 0.9$ ); and robust location- and scale-invariant transformation ( $\lambda = 0.4$ ,  $\sum r_i = 23.1$ ,  $\mu_{YJ} = 0.8$ ,  $\sigma_{YJ} = 0.8$ ).

Location- and scale-invariant transformation produced a lower overall residual sum, indicating a better transformation. Moreover, conventional transformations led to low standard deviation  $\sigma_{YJ}$  of the body mass feature after transformation. The empirical central normality test did not detect any statistically significant deviations from central normality for any transformation (all  $p \geq 0.38$ ).

#### 4.1.3. Latitude in the Ames housing dataset

Geospatial datasets usually contain coordinates. The Ames housing dataset contains data on 2930 properties that were sold between 2006 and 2010 (De Cock 2011), including their geospatial coordinates. The latitude was  $42.03 \pm 0.02$  (mean  $\pm$  standard deviation). Applying conventional and invariant Yeo-Johnson transformations to latitude yielded the following results,

see Figure 8: no transformation (residual sum  $\sum r_i = 328$ ); conventional transformation ( $\lambda = 62.1$ ,  $\sum r_i = 319$ ,  $\mu_{YJ} = 4.8 \cdot 10^{99}$ ,  $\sigma_{YJ} = 0.1 \cdot 10^{99}$ ); Raymaekers and Rousseeuw's robust adaptation ( $\lambda = 95.4$ ,  $\sum r_i = 319$ ,  $\mu_{YJ} = 6.4 \cdot 10^{153}$ ,  $\sigma_{YJ} = 0.3 \cdot 10^{153}$ ); location- and scale-invariant transformation ( $\lambda = 1.5$ ,  $\sum r_i = 326$ ,  $\mu_{YJ} = -1.2$ ,  $\sigma_{YJ} = 0.8$ ); and robust location- and scale-invariant transformation ( $\lambda = 1.4$ ,  $\sum r_i = 311$ ,  $\mu_{YJ} = -1.3$ ,  $\sigma_{YJ} = 0.9$ ).

Every transformation reduced the residual sum. The non-robust location- and scale-invariant transformation did not improve over conventional alternatives and yielded a data distribution lacking central normality (empirical central normality test:  $p = 0.05$ ). However, conventional transformations had high values for the  $\lambda$  parameter, which could lead to numerical issues.

#### 4.2. Robustness against outliers

We previously simulated data to assess invariant power transformations and their robustness against outliers. Here, we assess invariant power transformations in real data with outliers.

##### 4.2.1. Fuel efficiency in the Top Gear dataset

The Top Gear dataset contains data on 297 vehicles that appeared on the BBC television show *Top Gear* (Alfons 2021). Within this dataset, the fuel consumption feature contains outliers due to highly fuel-efficient vehicles. Applying conventional and invariant Yeo-Johnson transformations to the fuel consumption feature yielded the following results, see Figure 9: no transformation (residual sum  $\sum r_i = 54$ ,  $p = 0.76$ ); conventional transformation ( $\lambda = -0.1$ ,  $\sum r_i = 55$ ,  $\mu_{YJ} = 3.0$ ,  $\sigma_{YJ} = 0.3$ ,  $p = 0.01$ ); Raymaekers and Rousseeuw's robust adaptation ( $\lambda = 0.8$ ,  $\sum r_i = 48$ ,  $\mu_{YJ} = 29$ ,  $\sigma_{YJ} = 15$ ,  $p = 0.55$ ); location- and scale-invariant transformation ( $\lambda = -1.3$ ,  $\sum r_i = 44$ ,  $\mu_{YJ} = 0.5$ ,  $\sigma_{YJ} = 0.1$ ,  $p = 0.03$ ); and robust location- and scale-invariant transformation ( $\lambda = -0.9$ ,  $\sum r_i = 50$ ,  $\mu_{YJ} = 2.0$ ,  $\sigma_{YJ} = 2.3$ ,  $p = 0.58$ ).

Outliers cause non-robust transformations to fail to transform the data to a centrally normal distribution (empirical central normality test  $p = 0.01$  and  $p = 0.03$  for conventional and invariant transformations, respectively). Robust transformations produce distributions that are centrally normal (empirical central normality test  $p > 0.05$ ).

##### 4.2.2. Maximum arterial wall thickness in an ischemic stroke dataset

The ischemic stroke dataset contains historic data from 126 patients with risk at ischemic stroke (Kuhn and Johnson 2019). These patients under-

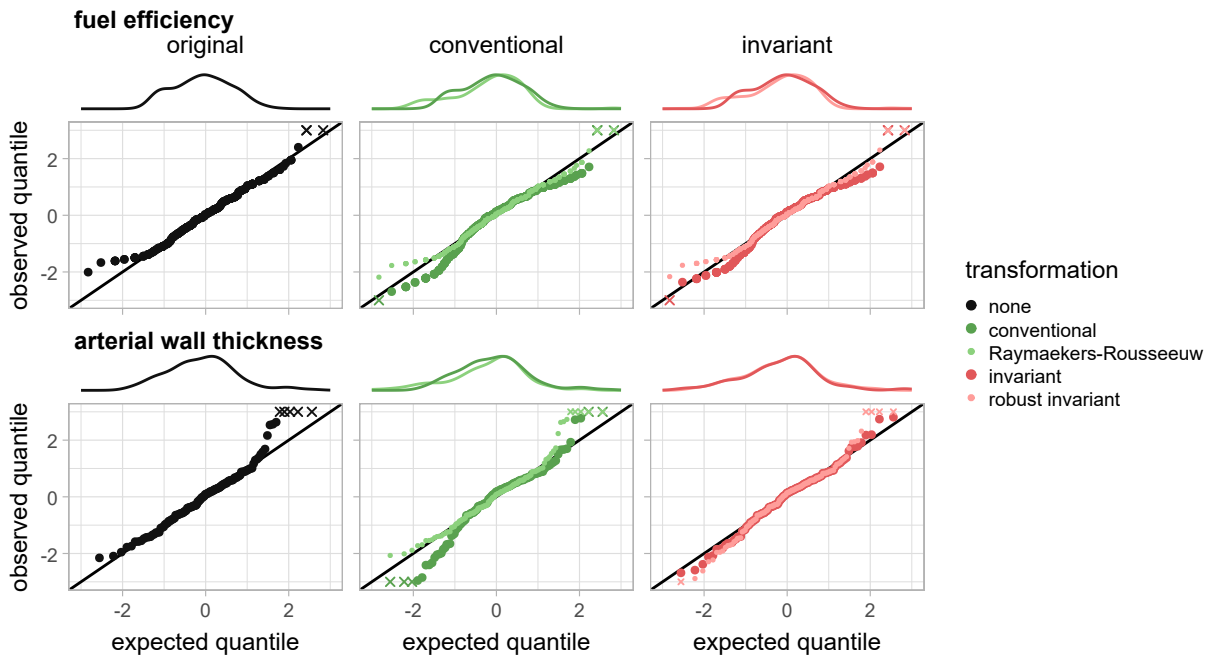


Figure 9: Quantile-quantile plots for two datasets with outliers: vehicle fuel consumption (top row), where outliers are related to highly fuel-efficient vehicles; and maximum arterial wall thickness in patients with ischemic stroke (bottom row). Multiple quantile-quantile plots are shown: for the original feature (left column); the feature transformed using the conventional Yeo-Johnson transformation and Raymaekers and Rousseeuw's robust adaptation (middle column); and the feature transformed using the non-robust and robust location- and scale invariant Yeo-Johnson transformations (right column). Samples with observed quantiles below  $-3.0$  or above  $3.0$  are indicated by crosses.

went Computed Tomography Angiography to characterize the carotid artery blockages. Angiography imaging was then assessed, and various characteristics related to the blood vessels and the disease are measured. The maximum arterial wall thickness feature contains several instances with outlier values. Applying conventional and invariant Yeo-Johnson transformations to this feature yielded the following results, see Figure 9: no transformation (residual sum  $\sum r_i = 110$ ,  $p = 0.56$ ); conventional transformation ( $\lambda = -0.7$ ,  $\sum r_i = 30$ ,  $\mu_{YJ} = 1.0$ ,  $\sigma_{YJ} = 0.1$ ,  $p = 0.01$ ); Raymaekers and Rousseeuw's robust adaptation ( $\lambda = 1.1$ ,  $\sum r_i = 136$ ,  $\mu_{YJ} = 7.2$ ,  $\sigma_{YJ} = 14$ ,  $p = 0.61$ ); location- and scale-invariant transformation ( $\lambda = 0.2$ ,  $\sum r_i = 12$ ,  $\mu_{YJ} = -11.8$ ,  $\sigma_{YJ} = 6.9$ ,  $p = 0.13$ ); and robust location- and scale-invariant transformation ( $\lambda = -0.6$ ,  $\sum r_i = 27$ ,  $\mu_{YJ} = 0.7$ ,  $\sigma_{YJ} = 0.1$ ,  $p = 0.10$ ).

Non-robust transformations failed to produce a centrally normal distribution (empirical central normality test  $p = 0.01$  and  $p = 0.02$  for conventional and invariant transformations, respectively). Robust transformations produce distributions that are centrally normal (empirical central normality test  $p > 0.05$ ).

#### *4.3. Integration into end-to-end machine learning*

We used 285 datasets from the Penn Machine Learning Benchmarks collection (Romano et al. 2022). In this collection, 122 datasets correspond to regression tasks and 163 datasets to classification tasks. Using the familiar auto-machine learning library (Zwanenburg and Löck 2024a) (version 1.5.0), each dataset was used to train a model for each of 16 process configurations. Each process configuration specifies the learner (generalised linear model or random forest), transformation method (none, conventional Yeo-Johnson, robust invariant Yeo-Johnson, robust invariant Yeo-Johnson with empirical central normality test (rejecting transformations with  $p \leq 0.01$ ), and normalisation method (none,  $z$ -standardisation), yielding 16 distinct configurations. Before each experiment, each dataset was randomly split into a training (70%) and holdout test (30%) set five times. Thus, a total of 22800 models were created. Each model was then evaluated using the holdout test set using one of two metrics, i.e. the root relative squared error (RRSE) for regression tasks and the area under the receiver operating characteristic curve (AUC) for classification tasks.

For the purpose of assessing the effect of the difficulty of the task, we computed the median performance score over all models for each dataset and assigned one the following categories:

- very easy:  $\text{AUC} \geq 0.90$  or  $\text{RRSE} \leq 0.10$  (87 datasets)
- easy:  $0.90 > \text{AUC} \geq 0.80$  or  $0.30 \geq \text{RRSE} > 0.10$  (46 datasets)
- intermediate:  $0.80 > \text{AUC} \geq 0.70$  or  $0.60 \geq \text{RRSE} > 0.30$  (72 datasets)
- difficult:  $0.70 > \text{AUC} \geq 0.60$  or  $0.80 \geq \text{RRSE} > 0.60$  (60 datasets)
- very difficult:  $0.60 > \text{AUC} \geq 0.50$  or  $1.00 \geq \text{RRSE} > 0.80$  (12 datasets)
- unsolvable:  $\text{AUC} < 0.50$  or  $\text{RRSE} > 1.00$  (8 datasets)

To remove the effect of the dataset, and allow for comparing metrics, we ranked all performance scores for each dataset so that a higher rank corresponds to better performance. Experiments yielding the same score received the same, average, rank. Subsequently ranks were normalised to the  $[0.0, 1.0]$  range.

Significant differences exist between process configurations (Friedman test:  $p < 10^{-8}$ ).

Here we focus on the subset of 232 datasets that contain numeric features. Considering single process parameters, the choice of learner (Wilcoxon signed rank test:  $p < 10^{-8}$ ) and normalisation method (Wilcoxon signed rank test:  $p = 0.007$ ) had a significant impact (at significance level  $p = 0.050$ ), but transformation method (Friedman test:  $p = 0.054$ ) did not.

To estimate the marginal effects of process parameters, including transformation method, we first fit a regression random forest (`ranger` package (Wright and Ziegler 2017) version 0.16.0): 2000 trees, minimum node size 2, other hyperparameters default) with process parameters and task difficulty as predictors and normalised rank as response variable. The estimated marginal effects are shown in Figure 10. On the scale of normalised ranks ( $[0.0, 1.0]$ ), the overall estimated marginal effect of using a random forest instead of generalised linear model was 0.272. The overall marginal effect of using z-standardisation to normalise features was 0.008. Transformation methods had the following marginal effects: 0.003 for using conventional Yeo-Johnson transformation instead of no transformation; -0.007 for using robust invariant Yeo-Johnson transformation instead of no transformation; -0.009 for using robust invariant Yeo-Johnson transformation with empirical central normality test instead of no transformation; -0.010 for using robust invariant Yeo-Johnson transformation instead of conventional Yeo-Johnson transformation; and -0.012 for using robust invariant Yeo-Johnson

transformation with empirical central normality test instead of conventional Yeo-Johnson transformation.

## 5. Discussion

In their work on power transformation, Box and Cox already mention transformation with a shift parameter, but preferred the version in Eq. 1 for the theoretical analysis in their paper (Box and Cox 1964), which subsequently became the convention. Yeo and Johnson’s power transformation lacks a shift parameter altogether (Yeo and Johnson 2000). We showed that these power transformations are sensitive to location and scale of data distributions. To mitigate this issue, we defined location- and scale-invariant variants of the Box-Cox and Yeo-Johnson transformations. We furthermore assessed methods for making these transformations robust to outliers, and devised an empirical test for central normality.

Robust location- and scale-invariant transformations are a suitable replacement for their conventional counterparts. They demonstrated robustness against outliers and prevent inaccurate transformations and potential numerical issues due to location and scale of the distribution of a feature. This is particularly relevant for automated data processing, where such issues may go unnoticed. Compared to non-robust location- and scale-invariant transformations, real-world examples with outliers showed higher residual errors of transformed features. Robust transformations seek to minimise residual errors for the central part of the distribution, instead of the entire distribution, including outliers. The empirical central normality test indicated that robust transformations are better able to achieve central normality in the presence of outliers. However, in a machine learning experiment of 232 real-world datasets that contained at least one numeric feature, we did not find a meaningful benefit – nor detriment – to model performance for location- and scale-invariant power transformations. One reason may be that numeric features with large location shifts ( $|\mu| > 1000.0$ ) were uncommon. Of the 4886 numeric features in the 232 datasets, 266 (5%) features in 34 datasets had large location shifts, of which 200 appeared in just 2 datasets. For the latter two datasets, the transformation method did not show significant difference between groups (Friedman test;  $p > 0.05$ ).

Location- and scale-invariant transformations are realised by simultaneously optimising three parameters, i.e. transformation parameter  $\lambda$ , shift parameter  $x_0$  and scale parameter  $s$ . We derived the log-likelihood func-

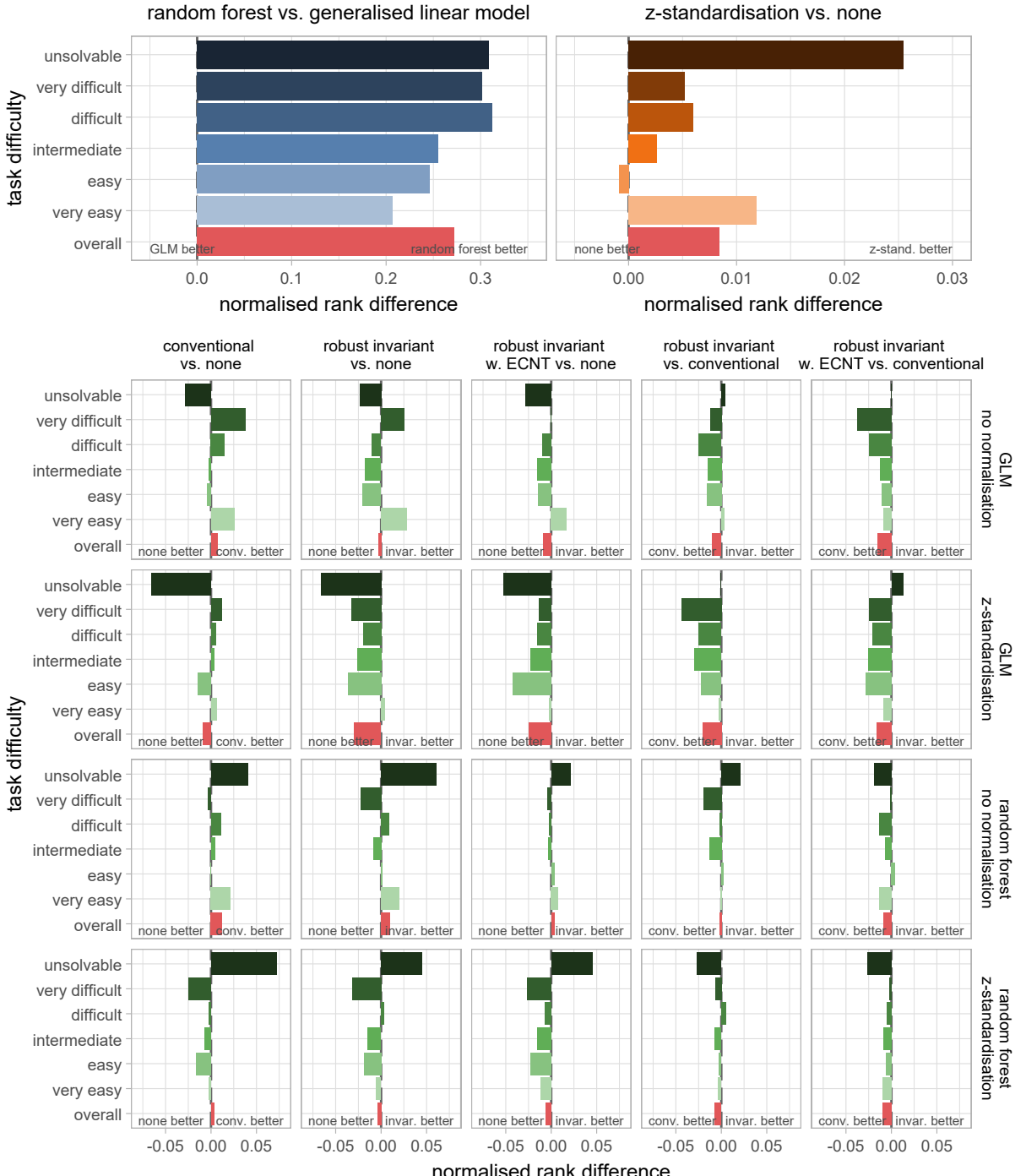


Figure 10: Estimated marginal effect of learners, normalisation and transformation methods on ranked model performance scores in 18560 machine learning experiments on 232 datasets. The top-left panel shows the marginal effect of learners, i.e. random forests and generalised linear models (GLM). Random forests outperform GLM models for all task difficulties. The top-right panel shows the marginal effect of feature normalisation methods, i.e. no normalisation and z-standardisation. z-standardisation is generally beneficial, but the estimated effect is negligible. The bottom panel shows the marginal effects of different transformation methods, split by learner and normalisation method. There is no consistent behaviour, and estimated effects are negligible. Note that the ranges of the  $x$ -axes of the three main panels differ. ECNT: empirical central normality test.

tion to facilitate optimisation using MLE. Alternatively, standardisation of a numeric variable (e.g., through subtracting its median value and division by its interquartile range) prior to conventional power transformations may achieve a similar effect in reducing sensitivity to the distribution’s location and scale. While this alternative helps prevent these issues – provided that normalisation does not lead to negative values for Box-Cox transformation – location- and scale-invariant transformations seem to provide an overall better transformation to normality (Appendix F).

We assessed several methods for robust power transformation. Methods that relied on the z-score of the transformed feature or the residual error yielded worse results than the non-robust method. This is partly due to the initial choice of threshold parameters. Using different initial values, closer to the upper limits ( $\delta_1 = 10.0$ ;  $\delta_2 = 10.0$ ), led to a reduced loss. However, these values effectively correspond to a non-robust transformation, where all instances receive the same weight. Underperformance of these methods could be explained by their use of transformed features for setting weights. Consequently, the weights change at each iteration in the MLE optimisation process. This increases local variance in the log-likelihood function and creates local optima that the optimiser may not handle well. As a consequence, optimal values for transformation parameter  $\lambda$  might differ, which increases the presented loss for optimising threshold parameters. Methods that relied on the empirical probability did not suffer from this issue, as weights remained fixed during MLE.

We introduced an empirical test for central normality to assess whether distributions deviate from normality in a way that might require closer inspection prior to further processing. The empirical test for central normality differs from other tests for normality, such as the Shapiro-Wilk test (Shapiro and Wilk 1965), in that the test statistic is independent of the number of samples. This makes this test more practical for assessing central normality for larger sample numbers, where other tests may detect inconsequential deviations from normality.

This work has the following limitations. Firstly, we did observe several numerical stability issues for optimisation criteria other than MLE (Appendix B). These appear in regions where transformation parameters would lead to very large or small numbers when using conventional power transformations. For MLE stability issues were not observed. Secondly, the empirical central normality test is based on simulations instead of statistical theory, and relies on a somewhat arbitrary definition of the central portion of a distri-

bution. Thus, while the test may assess whether data is sufficiently normally distributed for practical purposes, it should not be used as a strict test for normality.

## 6. Conclusion

Compared to their conventional versions, robust location- and scale-invariant Box-Cox and Yeo-Johnson transformations reduce sensitivity to outliers and the location and scale of features. An empirical central normality test can assess the quality of transformation of features to normal distributions. The combination of both facilitate the use of power transformations in automated data analysis workflows.

## 7. Data and code availability

Location- and scale-invariant power transformations were implemented in the `power.transform` package for R, which is available from GitHub (<https://github.com/oncoray/power.transform>) and the CRAN repository (<https://cran.r-project.org/package=power.transform>). The manuscript was created using R Markdown and is likewise available from the `power.transform` GitHub repository. Data and results for the machine learning experiment are separately available from Zenodo (<https://doi.org/10.5281/zenodo.13736671>).

## Appendix A. Log-likelihood functions for location and scale invariant power transformation

Location and scale-invariant Box-Cox and Yeo-Johnson transformations are parametrised using location  $x_0$  and scale  $s$  parameters, in addition to transformation parameter  $\lambda$ . This leads to the following transformations. The location and scale-invariant Box-Cox transformation is:

$$\phi_{BC}^{\lambda,x_0,s}(x_i) = \begin{cases} \left( \left( \frac{x_i - x_0}{s} \right)^\lambda - 1 \right) / \lambda & \text{if } \lambda \neq 0 \\ \log \left[ \frac{x_i - x_0}{s} \right] & \text{if } \lambda = 0 \end{cases} \quad (A.1)$$

where  $x_i - x_0 > 0$ . The location and scale-invariant Yeo-Johnson transformation is:

$$\phi_{\text{YJ}}^{\lambda, x_0, s}(x_i) = \begin{cases} \left( \left( 1 + \frac{x_i - x_0}{s} \right)^\lambda - 1 \right) / \lambda & \text{if } \lambda \neq 0 \text{ and } x_i - x_0 \geq 0 \\ \log \left[ 1 + \frac{x_i - x_0}{s} \right] & \text{if } \lambda = 0 \text{ and } x_i - x_0 \geq 0 \\ - \left( \left( 1 - \frac{x_i - x_0}{s} \right)^{2-\lambda} - 1 \right) / (2 - \lambda) & \text{if } \lambda \neq 2 \text{ and } x_i - x_0 < 0 \\ - \log \left[ 1 - \frac{x_i - x_0}{s} \right] & \text{if } \lambda = 2 \text{ and } x_i - x_0 < 0 \end{cases} \quad (\text{A.2})$$

The parameters of these power transformations can be optimised based by maximising the log-likelihood function, under the assumption that the transformed feature  $\phi^{\lambda, x_0, s}(\mathbf{X})$  follows a normal distribution. The log-likelihood functions for conventional Box-Cox and Yeo-Johnson transformations are well-known. However, the introduction of scaling parameter  $s$  prevents their direct use. Here, we first derive the general form of the log-likelihood functions, and then derive their power-transformation specific definitions.

Let  $f(x_1, \dots, x_n)$  be the probability density function of feature  $\mathbf{X} = \{x_1, \dots, x_n\}$ , and  $f^{\lambda, x_0, s}(\phi^{\lambda, x_0, s}(x_1), \dots, \phi^{\lambda, x_0, s}(x_n))$  be the probability density function of the transformed feature  $\phi^{\lambda, x_0, s}(\mathbf{X})$ , that is assumed to follow a normal distribution.

The two probability density functions are related as follows:

$$f^{\lambda, x_0, s}(x_1, \dots, x_n) = f^{\lambda, x_0, s}(\phi^{\lambda, x_0, s}(x_1), \dots, \phi^{\lambda, x_0, s}(x_n)) |\mathbf{J}| \quad (\text{A.3})$$

Where,  $|\mathbf{J}|$  is the determinant of Jacobian  $\mathbf{J}$ . The Jacobian takes the following form, with off-diagonal elements 0:

$$\mathbf{J} = \begin{bmatrix} \frac{\partial}{\partial x_1} \phi^{\lambda, x_0, s}(x_1) & 0 & \dots & 0 \\ 0 & \frac{\partial}{\partial x_2} \phi^{\lambda, x_0, s}(x_2) & \dots & 0 \\ \vdots & \vdots & \ddots & \vdots \\ 0 & 0 & 0 & \frac{\partial}{\partial x_n} \phi^{\lambda, x_0, s}(x_n) \end{bmatrix} \quad (\text{A.4})$$

Thus,  $|\mathbf{J}| = \prod_{i=1}^n \frac{\partial}{\partial x_i} \phi^{\lambda, x_0, s}(x_i)$ .

Since in our situation  $\{x_1, \dots, x_n\}$  in  $f^{\lambda, x_0, s}(x_1, \dots, x_n)$  are considered fixed (i.e., known),  $f^{\lambda, x_0, s}(x_1, \dots, x_n)$  may be considered a likelihood function. The log-likelihood function  $\hat{\gamma}^{\lambda, x_0, s}$  is then:

$$\begin{aligned}
\hat{\downarrow}^{\lambda, x_0, s} &= \log f^{\lambda, x_0, s}(x_1, \dots, x_n) \\
&= \log [f^{\lambda, x_0, s}(\phi^{\lambda, x_0, s}(x_1), \dots, \phi^{\lambda, x_0, s}(x_n))] + \log |\mathbf{J}| \\
&= \log [f^{\lambda, x_0, s}(\phi^{\lambda, x_0, s}(x_1), \dots, \phi^{\lambda, x_0, s}(x_n))] + \log \prod_{i=1}^n \frac{\partial}{\partial x_i} \phi^{\lambda, x_0, s}(x_i) \\
&= -\frac{n}{2} \log [2\pi\sigma^2] - \frac{1}{2\sigma^2} \sum_{i=1}^n (\phi^{\lambda, x_0, s}(x_i) - \mu)^2 + \sum_{i=1}^n \log \left[ \frac{\partial}{\partial x_i} \phi^{\lambda, x_0, s}(x_i) \right]
\end{aligned} \tag{A.5}$$

With  $\mu$  the average of  $\phi^{\lambda, x_0, s}(\mathbf{X})$  and  $\sigma^2$  its variance. The first two terms derive directly from the log-likelihood function of a normal distribution, and are not specific to the type of power transformation used. However, the final term differs between Box-Cox and Yeo-Johnson transformations.

#### *Appendix A.1. Location- and scale-invariant Box-Cox transformation*

For the location- and scale-invariant Box-Cox transformation the partial derivative is:

$$\begin{aligned}
\frac{\partial}{\partial x_i} \phi_{\text{BC}}^{\lambda, x_0, s}(x_i) &= \frac{1}{s} \left( \frac{x_i - x_0}{s} \right)^{\lambda-1} \\
&= \frac{1}{s^\lambda} (x_i - x_0)^{\lambda-1}
\end{aligned} \tag{A.6}$$

Thus the final term in  $\hat{\downarrow}_{\text{BC}}^{\lambda, x_0, s}$  is:

$$\begin{aligned}
\sum_{i=1}^n \log \frac{\partial}{\partial x_i} \phi_{\text{BC}}^{\lambda, x_0, s}(x_i) &= \sum_{i=1}^n \log [s^{-\lambda} (x_i - x_0)^{\lambda-1}] \\
&= \sum_{i=1}^n \log [s^{-\lambda}] + \log [(x_i - x_0)^{\lambda-1}] \\
&= -n\lambda \log s + (\lambda - 1) \sum_{i=1}^n \log [x_i - x_0]
\end{aligned} \tag{A.7}$$

This leads to the following log-likelihood:

$$\hat{\psi}_{\text{BC}}^{\lambda, x_0, s} = -\frac{n}{2} \log [2\pi\sigma^2] - \frac{1}{2\sigma^2} \sum_{i=1}^n (\phi^{\lambda, x_0, s}(x_i) - \mu)^2 - n\lambda \log s + (\lambda - 1) \sum_{i=1}^n \log [x_i - x_0] \quad (\text{A.8})$$

Similarly to Raymaekers and Rousseeuw (2024), sample weights  $w_i$  are introduced to facilitate robust power transformations. The weighted log-likelihood of the location- and scale-invariant Box-Cox transformation is:

$$\hat{\psi}_{\text{rBC}}^{\lambda, x_0, s} = -\frac{1}{2} \left( \sum_{i=1}^n w_i \right) \log [2\pi\sigma_w^2] - \frac{1}{2\sigma_w^2} \sum_{i=1}^n w_i (\phi^{\lambda, x_0, s}(x_i) - \mu_w)^2 - \lambda \left( \sum_{i=1}^n w_i \right) \log s + (\lambda - 1) \sum_{i=1}^n w_i \log [x_i - x_0] \quad (\text{A.9})$$

where  $\mu_w$  and  $\sigma_w^2$  are the weighted mean and weighted variance of the Box-Cox transformed feature  $\phi_{\text{BC}}^{\lambda, x_0, s}(\mathbf{X})$ , respectively:

$$\sigma_w^2 = \frac{\sum_{i=1}^n w_i (\phi_{\text{BC}}^{\lambda, x_0, s}(x_i) - \mu_w)^2}{\sum_{i=1}^n w_i} \quad \text{with } \mu_w = \frac{\sum_{i=1}^n \phi_{\text{BC}}^{\lambda, x_0, s}(x_i)}{\sum_{i=1}^n w_i} \quad (\text{A.10})$$

#### Appendix A.2. Location- and scale-invariant Yeo-Johnson transformation

For the location- and scale-invariant Yeo-Johnson transformation, the partial derivative is:

$$\frac{\partial}{\partial x_i} \phi_{\text{YJ}}^{\lambda, x_0, s}(x_i) = \begin{cases} \frac{1}{s} \left(1 + \frac{x_i - x_0}{s}\right)^{\lambda-1} & \text{if } x_i - x_0 \geq 0 \\ \frac{1}{s} \left(1 - \frac{x_i - x_0}{s}\right)^{1-\lambda} & \text{if } x_i - x_0 < 0 \end{cases} \quad (\text{A.11})$$

Thus the final term in  $\hat{\psi}_{\text{YJ}}^{\lambda, x_0, s}$  is:

$$\sum_{i=1}^n \log \frac{\partial}{\partial x_i} \phi_{\text{YJ}}^{\lambda, x_0, s}(x_i) = -n \log s + (\lambda - 1) \sum_{i=1}^n \text{sgn}(x_i - x_0) \log \left[ 1 + \frac{|x_i - x_0|}{s} \right] \quad (\text{A.12})$$

This leads to the following log-likelihood:

$$\begin{aligned}\hat{\psi}_{YJ}^{\lambda,x_0,s} = & -\frac{n}{2} \log [2\pi\sigma^2] - \frac{1}{2\sigma^2} \sum_{i=1}^n (\phi^{\lambda,x_0,s}(x_i) - \mu)^2 \\ & - n \log s + (\lambda - 1) \sum_{i=1}^n \operatorname{sgn}(x_i - x_0) \log \left[ 1 + \frac{|x_i - x_0|}{s} \right]\end{aligned}\quad (\text{A.13})$$

The weighted log-likelihood for location- and scale-invariant Yeo-Johnson transformation is:

$$\begin{aligned}\hat{\psi}_{rYJ}^{\lambda,x_0,s} = & -\frac{1}{2} \left( \sum_{i=1}^n w_i \right) \log [2\pi\sigma_w^2] - \frac{1}{2\sigma_w^2} \sum_{i=1}^n w_i (\phi^{\lambda,x_0,s}(x_i) - \mu_w)^2 \\ & - \left( \sum_{i=1}^n w_i \right) \log s + (\lambda - 1) \sum_{i=1}^n w_i \operatorname{sgn}(x_i - x_0) \log \left[ 1 + \frac{|x_i - x_0|}{s} \right]\end{aligned}\quad (\text{A.14})$$

where  $\mu_w$  and  $\sigma_w^2$  are the weighted mean and weighted variance of the Yeo-Johnson transformed feature  $\phi_{YJ}^{\lambda,x_0,s}(\mathbf{X})$ :

$$\sigma_w^2 = \frac{\sum_{i=1}^n w_i (\phi_{YJ}^{\lambda,x_0,s}(x_i) - \mu_w)^2}{\sum_{i=1}^n w_i} \quad \text{with } \mu_w = \frac{\sum_{i=1}^n \phi_{YJ}^{\lambda,x_0,s}(x_i)}{\sum_{i=1}^n w_i} \quad (\text{A.15})$$

## Appendix B. Optimisation of transformation parameters

Maximum likelihood estimation (MLE) is commonly used to optimise parameters for power transformation. Generally, optimisation requires minimisation or maximisation of a criterion. In MLE, the maximised criterion is the log-likelihood function of the normal distribution. Here, we investigate power transformation using optimisation criteria that are closely related to test statistics for normality tests.

Let  $\mathbf{X}$  be a feature with ordered feature values, and  $\mathbf{Y}^\lambda = \phi^\lambda(\mathbf{X})$  and  $\mathbf{Y}^{\lambda,x_0,s} = \phi^{\lambda,x_0,s}(\mathbf{X})$  its transformed values using conventional and shift and scale invariant power transformations, respectively. Since power transformations are monotonic,  $\mathbf{Y}$  will likewise be ordered.

Below we will focus on criteria based on the empirical density function and those based on skewness and kurtosis of the transformed features. Other potential criteria, such as the Shapiro-Wilk test statistic (Shapiro and Wilk 1965) are not investigated here. In the case of the Shapiro-Wilk test statistic this is because of lack of scalability to features with many ( $> 5000$ ) instances, and because adapting the test statistic to include weights is not straightforward.

### *Appendix B.1. Empirical density function-based criteria*

The first class of criteria is based on the empirical distribution function (EDF). Transformation parameters are then fit through minimisation of the distance between the empirical distribution function  $F_\epsilon$  and the cumulative density function (CDF) of the normal distribution  $F_N$ . Let  $F_\epsilon(x_i) = \frac{i-1/3}{n+1/3}$  be the empirical probability of instance  $i$ . The normal distribution is parametrised by location parameter  $\mu$  and scale parameter  $\sigma$ , both of which have to be estimated from the data. For non-robust power transformations,  $\mu$  and  $\sigma$  are sample mean and sample standard deviation, respectively. For robust power transformations, we estimate  $\mu$  and  $\sigma$  as Huber M-estimates of location and scale of the transformed feature  $\phi^{\lambda, x_0, s}(\mathbf{X})$  (Huber 1981).

#### *Appendix B.1.1. Anderson-Darling criterion*

The Anderson-Darling criterion is based on the empirical distribution function of  $\mathbf{X}$ . We define this criterion as follows:

$$U_{AD}(\mathbf{X}, \lambda, x_0) = \frac{1}{\sum_{i=1}^n w_i} \sum_{i=1}^n w_i \frac{(F_\epsilon(x_i) - F_N(\phi^{\lambda, x_0, s}(x_i); \mu, \sigma))^2}{F_N(\phi^{\lambda, x_0, s}(x_i); \mu, \sigma)(1 - F_N(\phi^{\lambda, x_0, s}(x_i); \mu, \sigma))} \quad (\text{B.1})$$

Here  $w_i$  are weights, and  $\mu$  and  $\sigma$  are location and scale parameters. For non-robust power transformations, all  $w_i = 1$ . Note that this criterion is not the same as the Anderson-Darling test statistic (Anderson and Darling 1952), which involves solving (or approximating) an integral function, contains an extra scalar multiplication term, and does not include weights. The Anderson-Darling criterion seeks to minimise the squared Euclidean distance between the EDF and the normal CDF, with differences at the upper and lower end of the normal CDF receiving more weight than those at the centre of the CDF.

### Appendix B.1.2. Cramér-von Mises criterion

The Cramér-von Mises criterion is also based on the empirical distribution function of  $\mathbf{X}$ . We define the Cramér-von Mises criterion as follows:

$$U_{\text{CvM}}(\mathbf{X}, \lambda, x_0) = \frac{1}{\sum_{i=1}^n w_i} \sum_{i=1}^n w_i (F_\epsilon(x_i) - F_N(\phi^{\lambda, x_0, s}(x_i); \mu, \sigma))^2 \quad (\text{B.2})$$

Here  $w_i$  are weights, and  $\mu$  and  $\sigma$  are location and scale parameters. For non-robust power transformations, all  $w_i = 1$ . The criterion is similar to the Cramér-von Mises test statistic Mises (1928), aside from a additive scalar value and the introduction of weights. This criterion, like the Anderson-Darling criterion, seeks to minimise the squared Euclidean distance between the EDF and the normal CDF. Unlike the Anderson-Darling criterion, this criterion weights all instances equally.

For conventional power transformations with a fixed shift parameter, the transformation  $\phi^{\lambda, x_0, s}(\mathbf{X})$  may be substituted by  $\phi^\lambda(\mathbf{X})$  in the definition of the Cramér-von Mises criterion.

### Appendix B.2. Skewness-kurtosis-based criteria

The second class of criteria seeks to reduce skewness and (excess) kurtosis of the transformed feature  $\mathbf{Y}$ . We will first define the location  $\mu$  and scale  $\sigma$  of the the transformed as these are required for computing skewness and kurtosis. Here,  $\mu$  is defined as:

$$\mu = \frac{\sum_{i=1}^n \phi^{\lambda, x_0, s}(x_i)}{\sum_{i=1}^n w_i} \quad (\text{B.3})$$

The location, or mean, is weighted using weights  $w_i$ . For non-robust transformations,  $w_i = 1$ . Then,  $\sigma^2$  is defined as:

$$\sigma^2 = \frac{\sum_{i=1}^n w_i (\phi^{\lambda, x_0, s}(x_i) - \mu)^2}{\sum_{i=1}^n w_i} \quad (\text{B.4})$$

Skewness is defined as:

$$s = \frac{\sum_{i=1}^n w_i (\phi^{\lambda, x_0, s}(x_i) - \mu)^3}{\sigma^3 \sum_{i=1}^n w_i} \quad (\text{B.5})$$

Kurtosis is defined as:

$$k = \frac{\sum_{i=1}^n w_i (\phi^{\lambda, x_0, s}(x_i) - \mu)^4}{\sigma^4 \sum_{i=1}^n w_i} \quad (\text{B.6})$$

### Appendix B.2.1. D'Agostino criterion

The D'Agostino criterion defined here follows the D'Agostino  $K^2$  test statistic (D'Agostino and Belanger 1990). This test statistic is composed of two separate test statistics, one of which is related to skewness, and the other to kurtosis. Both test statistics are computed in several steps. Let us first define  $\nu = \sum_{i=1}^n w_i$ . Thus for non-robust power transformations,  $\nu = n$ .

For the skewness test statistic we first compute (D'Agostino and Belanger 1990):

$$\beta_1 = s \sqrt{\frac{(\nu + 1)(\nu + 3)}{6(\nu - 2)}} \quad (\text{B.7})$$

$$\beta_2 = 3 \frac{(\nu^2 + 27\nu - 70)(\nu + 1)(\nu + 3)}{(\nu - 2)(\nu + 5)(\nu + 7)(\nu + 9)} \quad (\text{B.8})$$

$$\alpha = \sqrt{\frac{2}{\sqrt{2\beta_2 - 2} - 2}} \quad (\text{B.9})$$

$$\delta = \frac{1}{\sqrt{\log \left[ \sqrt{-1 + \sqrt{2 * \beta_2 - 2}} \right]}} \quad (\text{B.10})$$

The skewness test statistic is then:

$$Z_s = \delta \log \left[ \frac{\beta_1}{\alpha} + \sqrt{\frac{\beta_1^2}{\alpha^2} + 1} \right] \quad (\text{B.11})$$

For the kurtosis test statistic we first compute (D'Agostino and Belanger 1990; Anscombe and Glynn 1983):

$$\beta_1 = 3 \frac{\nu - 1}{\nu + 1} \quad (\text{B.12})$$

$$\beta_2 = 24\nu \frac{(\nu - 2)(\nu - 3)}{(\nu + 1)^2(\nu + 3)(\nu + 5)} \quad (\text{B.13})$$

$$\beta_3 = 6 \frac{\nu^2 - 5\nu + 2}{(\nu + 7)(\nu + 9)} \sqrt{6 \frac{(\nu + 3)(\nu + 5)}{\nu(\nu - 2)(\nu - 3)}} \quad (\text{B.14})$$

$$\alpha_1 = 6 + \frac{8}{\beta_3} \left[ \frac{2}{\beta_3} + \sqrt{1 + \frac{4}{\beta_3^2}} \right] \quad (\text{B.15})$$

$$\alpha_2 = \frac{k - \beta_1}{\sqrt{\beta_2}} \quad (\text{B.16})$$

The kurtosis test statistic is then:

$$Z_k = \sqrt{\frac{9\alpha_1}{2}} \left[ 1 - \frac{2}{9\alpha_1} - \left( \frac{1 - 2/\alpha_1}{1 + \alpha_2 \sqrt{2/(\alpha_1 - 4)}} \right)^{1/3} \right] \quad (\text{B.17})$$

The D'Agostino  $K^2$  test statistic and our criterion are the same, and are defined as:

$$U_{\text{DA}}(\mathbf{X}, \lambda, x_0) = Z_s^2 + Z_k^2 \quad (\text{B.18})$$

The main difference between the test statistic as originally formulated, and the criterion proposed here is the presence of weights for robust power transformation.

#### *Appendix B.2.2. Jarque-Bera criterion*

The second criterion based on skewness and kurtosis is the Jarque-Bera criterion. It is relatively simple to compute compared to the D'Agostino criterion:

$$U_{\text{JB}}(\mathbf{X}, \lambda, x_0) = s^2 + (k - 3)^2 / 4 \quad (\text{B.19})$$

The main difference between the above criterion and the Jarque-Bera test statistic (Jarque and Bera 1980) is that a scalar multiplication is absent.

#### *Appendix B.3. Optimisation using non-MLE criteria*

Each of the above criteria can be used for optimisation, i.e.:

$$\left\{ \hat{\lambda}, \hat{x}_0, \hat{s}_0 \right\} = \underset{\lambda, x_0, s}{\operatorname{argmin}} U(\mathbf{X}, \lambda, x_0, s) \quad (\text{B.20})$$

For conventional power transformations with fixed location and scale parameters, the transformation  $\phi^{\lambda, x_0, s}(\mathbf{X})$  may be substituted by  $\phi^\lambda(\mathbf{X})$ , or equivalently,  $x_0$  and  $s$  may be fixed:

$$\left\{ \hat{\lambda} \right\} = \underset{\lambda}{\operatorname{argmin}} U(\mathbf{X}, \lambda; x_0, s) \quad (\text{B.21})$$

### Appendix C. Simulations with other optimisation criteria

Invariance of location- and scale-invariant power transformations was assessed using the optimisation criteria in Appendix B. This follows the simulation in section 3.1, where MLE was used for optimization. In short, we first randomly drew 10000 values from a normal distribution:  $\mathbf{X}_{\text{normal}} = \{x_1, x_2, \dots, x_{10000}\} \sim \mathcal{N}(0, 1)$ , or equivalently  $\mathbf{X}_{\text{normal}} = \{x_1, x_2, \dots, x_{10000}\} \sim \mathcal{AGN}(0, 1/\sqrt{2}, 0.5, 2)$ . The second distribution was a right-skewed normal distribution  $\mathbf{X}_{\text{right}} = \{x_1, x_2, \dots, x_{10000}\} \sim \mathcal{AGN}(0, 1/\sqrt{2}, 0.2, 2)$ . The third distribution was a left-skewed normal distribution  $\mathbf{X}_{\text{left}} = \{x_1, x_2, \dots, x_{10000}\} \sim \mathcal{AGN}(0, 1/\sqrt{2}, 0.8, 2)$ . We then computed transformation parameter  $\lambda$  using the original definitions (equations 1 and 2) and the location- and scale-invariant definitions (equations 3 and 4) for each distribution using different optimisation criteria. To assess location invariance, a positive value  $d_{\text{shift}}$  was added to each distribution with  $d_{\text{shift}} \in [1, 10^6]$ . Similarly, to assess scale invariance, each distribution was multiplied by a positive value  $d_{\text{scale}}$ , where  $d_{\text{scale}} \in [1, 10^6]$ .

The results are shown in Figure C.11.

### Appendix D. Experimental results using location- and scale-invariant Box-Cox transformation

The effect of using location- and scale-invariant transformations was investigated using real-world datasets.

#### *Appendix D.1. Invariance*

Results for Box-Cox transformations of features without outliers are shown in Figure D.12.

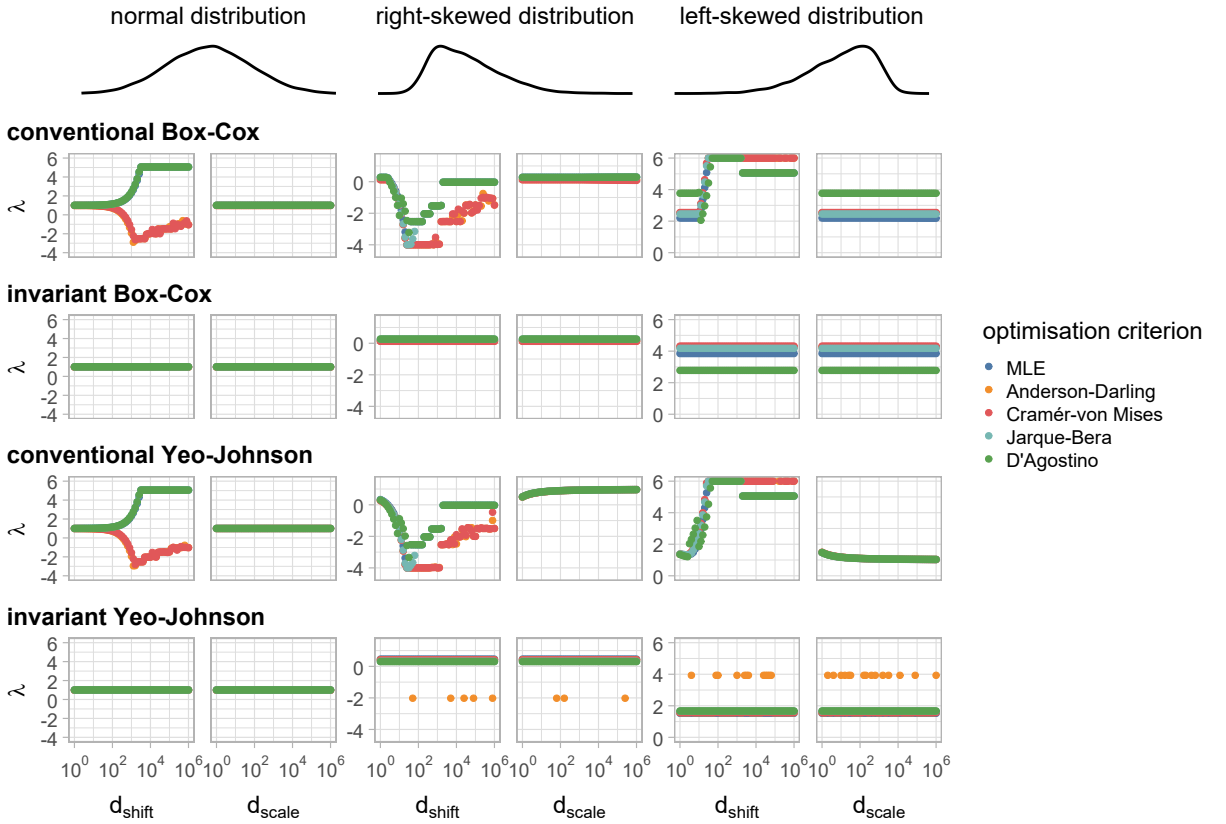


Figure C.11: Invariant power transformation produces transformation parameters that are invariant to location and scale. Samples were drawn from normal, right-skewed and left-skewed distributions, respectively, which then underwent a shift  $d_{\text{shift}}$  or multiplication by  $d_{\text{scale}}$ . Estimates of the transformation parameter  $\lambda$  for the conventional power transformations show strong dependency on the overall location and scale of the distribution and the optimisation criterion, whereas estimates obtained for the location- and scale-invariant power transformations are constant. For location- and scale-invariant power transformations, the Anderson-Darling criterion leads to unstable estimates of  $\lambda$  for skewed distributions, possibly due to large weights being assigned to samples at the upper and lower ends of the distribution.

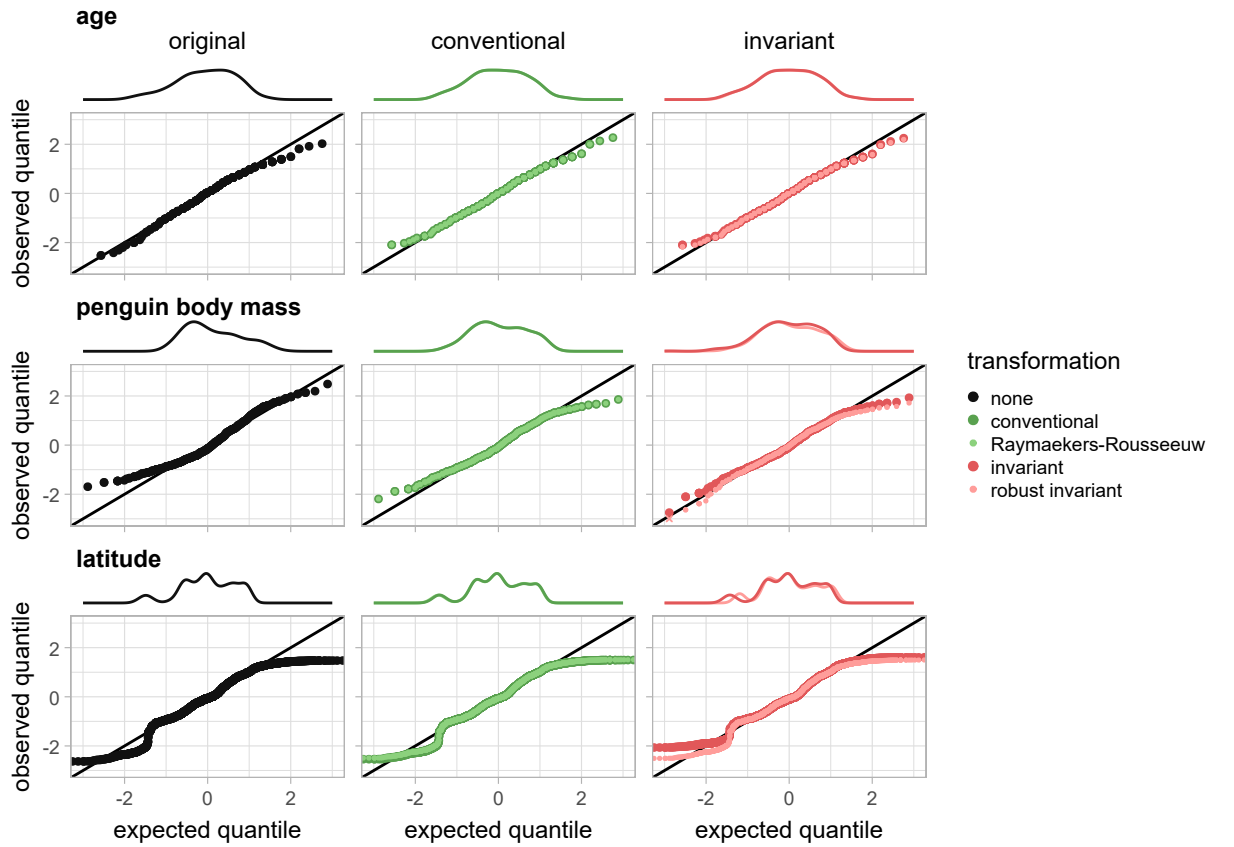


Figure D.12: Quantile-quantile plots for several datasets: age of patients with lung cancer (top row); penguin body mass (middle row); and latitude coordinates of houses sold in Ames, Iowa (bottom row). Multiple quantile-quantile plots are shown: for the original feature (left column); the feature transformed using the conventional Box-Cox transformation and Raymaekers and Rousseeuw's robust adaptation (middle column); and the feature transformed using the non-robust and robust location- and scale invariant Box-Cox transformations (right column).

#### *Appendix D.1.1. Age of patients with lung cancer*

Applying conventional and invariant Box-Cox transformations to age of patients with lung cancer (Loprinzi et al. 1994) yielded the following results: no transformation (sum of residuals with normal distribution  $\sum r_i = 16.5$ ); conventional transformation ( $\lambda = 1.9$ ,  $\sum r_i = 11.5$ ,  $\mu_{BC} = 1.6 \cdot 10^3$ ,  $\sigma_{BC} = 0.4 \cdot 10^3$ ); Raymaekers and Rousseeuw's robust adaptation ( $\lambda = 1.9$ ,  $\sum r_i = 11.5$ ,  $\mu_{BC} = 1.6 \cdot 10^3$ ,  $\sigma_{BC} = 0.4 \cdot 10^3$ ); location- and scale-invariant transformation ( $\lambda = 1.7$ ,  $\sum r_i = 11.6$ ,  $\mu_{BC} = 1.9$ ,  $\sigma_{BC} = 0.8$ ); and robust location- and scale-invariant transformation ( $\lambda = 1.5$ ,  $\sum r_i = 11.6$ ,  $\mu_{BC} = 3.6$ ,  $\sigma_{BC} = 1.2$ ).

Compared to location- and scale-invariant Yeo-Johnson transformations, the Box-Cox transformations do not reduce residuals compared to conventional variants.

#### *Appendix D.1.2. Penguin body mass*

Applying conventional and invariant Box-Cox transformations to the body mass of penguins (Gorman, Williams, and Fraser 2014) yielded the following results: no transformation (residual sum  $\sum r_i = 48.0$ ); conventional transformation ( $\lambda = -0.5$ ,  $\sum r_i = 32.2$ ,  $\mu_{BC} = 2.1$ ,  $\sigma_{BC} = 4 \cdot 10^{-3}$ ); Raymaekers and Rousseeuw's robust adaptation ( $\lambda = -0.5$ ,  $\sum r_i = 32.2$ ,  $\mu_{BC} = 2.1$ ,  $\sigma_{BC} = 4 \cdot 10^{-3}$ ); location- and scale-invariant transformation ( $\lambda = 0.5$ ,  $\sum r_i = 27.3$ ,  $\mu_{BC} = 0.3$ ,  $\sigma_{BC} = 0.6$ ); and robust location- and scale-invariant transformation ( $\lambda = 0.2$ ,  $\sum r_i = 25.2$ ,  $\mu_{BC} = 0.4$ ,  $\sigma_{BC} = 0.6$ ).

Just as for location- and scale-invariant Yeo-Johnson transformations, Box-Cox transformations produced a lower overall residual sum compared to their conventional counterparts. Similarly, conventional transformations led to low standard deviation  $\sigma_{YJ}$  of the body mass feature after transformation.

#### *Appendix D.1.3. Latitude in the Ames housing dataset*

Applying conventional and invariant Box-Cox transformations to the latitude of houses in the Ames housing dataset (De Cock 2011) yielded the following results: no transformation (residual sum  $\sum r_i = 328$ ); conventional transformation ( $\lambda = 62.1$ ,  $\sum r_i = 319$ ,  $\mu_{BC} = 1.1 \cdot 10^{99}$ ,  $\sigma_{BC} = 0.0 \cdot 10^{99}$ ); Raymaekers and Rousseeuw's robust adaptation ( $\lambda = 96.0$ ,  $\sum r_i = 319$ ,  $\mu_{BC} = 6.2 \cdot 10^{153}$ ,  $\sigma_{BC} = 0.3 \cdot 10^{153}$ ); location- and scale-invariant transformation ( $\lambda = 1.9$ ,  $\sum r_i = 312$ ,  $\mu_{BC} = 2.3$ ,  $\sigma_{BC} = 0.9$ ); and robust location- and scale-invariant transformation ( $\lambda = 1.2$ ,  $\sum r_i = 316$ ,  $\mu_{BC} = 5.5$ ,  $\sigma_{BC} = 1.4$ ).

Similar to conventional Yeo-Johnson transformations (non-robust and robust), conventional Box-Cox transformations had high values for the  $\lambda$  parameter, which could lead to numerical issues. Location- and scale-invariant Box-Cox transformations did not suffer from this issue.

#### *Appendix D.2. Robustness against outliers*

Results for Box-Cox transformations of features with outliers are shown in Figure D.13.

##### *Appendix D.2.1. Fuel efficiency in the Top Gear dataset*

The Top Gear dataset contains data on 297 vehicles, with outliers related highly fuel-efficient vehicles (Alfons 2021). Applying conventional and invariant Box-Cox transformations to the fuel consumption feature yielded the following results: no transformation (residual sum  $\sum r_i = 54$ ,  $p = 0.76$ ); conventional transformation ( $\lambda = -0.1$ ,  $\sum r_i = 55$ ,  $\mu_{BC} = 3.0$ ,  $\sigma_{BC} = 0.3$ ,  $p = 0.01$ ); Raymaekers and Rousseeuw's robust adaptation ( $\lambda = 0.8$ ,  $\sum r_i = 48$ ,  $\mu_{BC} = 29$ ,  $\sigma_{BC} = 15$ ,  $p = 0.55$ ); location- and scale-invariant transformation ( $\lambda = -0.7$ ,  $\sum r_i = 44$ ,  $\mu_{BC} = 0.6$ ,  $\sigma_{BC} = 0.2$ ,  $p = 0.02$ ); and robust location- and scale-invariant transformation ( $\lambda = 1.1$ ,  $\sum r_i = 59$ ,  $\mu_{BC} = 2.4$ ,  $\sigma_{BC} = 1.8$ ,  $p = 0.83$ ).

##### *Appendix D.2.2. Maximum arterial wall thickness in an ischemic stroke dataset*

The ischemic stroke dataset contains historic data from 126 patients with risk at ischemic stroke (Kuhn and Johnson 2019). Applying conventional and invariant Box-Cox transformations to the maximum arterial wall thickness feature yielded the following results: no transformation (residual sum  $\sum r_i = 110$ ,  $p = 0.56$ ); conventional transformation ( $\lambda = -0.5$ ,  $\sum r_i = 33$ ,  $\mu_{BC} = 1.0$ ,  $\sigma_{BC} = 0.2$ ,  $p = 0.01$ ); Raymaekers and Rousseeuw's robust adaptation ( $\lambda = 1.1$ ,  $\sum r_i = 127$ ,  $\mu_{BC} = 5.5$ ,  $\sigma_{BC} = 12$ ,  $p = 0.60$ ); location- and scale-invariant transformation ( $\lambda = -1.0$ ,  $\sum r_i = 28$ ,  $\mu_{BC} = 0.7$ ,  $\sigma_{BC} = 0.1$ ,  $p = 0.01$ ); and robust location- and scale-invariant transformation ( $\lambda = 0.5$ ,  $\sum r_i = 56$ ,  $\mu_{BC} = 2.2$ ,  $\sigma_{BC} = 1.4$ ,  $p = 0.35$ ).

## **Appendix E. Empirical central normality test**

The empirical central normality test was derived using data sampled from asymmetric generalised normal distributions, including outliers, to resemble more realistic datasets. Here we assess the type I error rate of two, less realistic, sets of data:

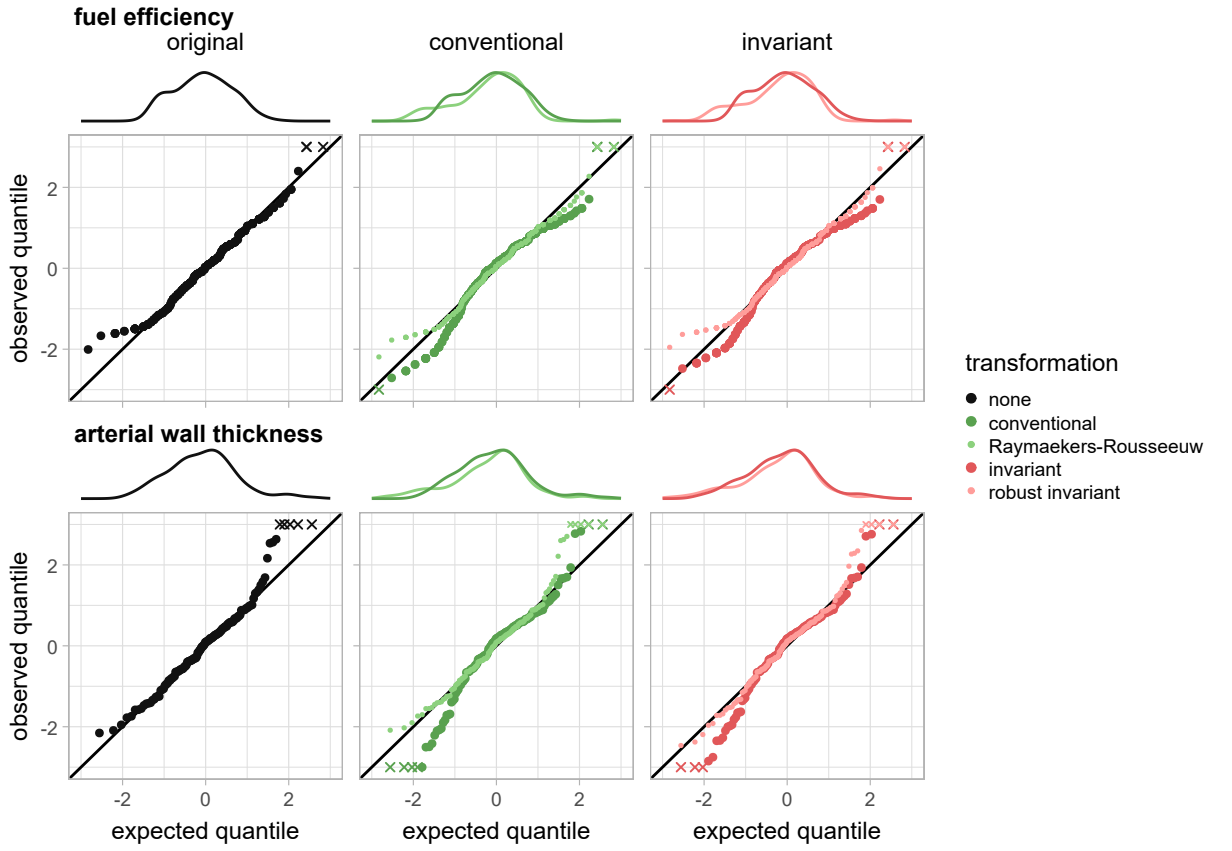


Figure D.13: Quantile-quantile plots for two datasets with outliers: vehicle fuel consumption (top row), where outliers are related to highly fuel-efficient vehicles; and maximum arterial wall thickness in patients with ischemic stroke (bottom row). Multiple quantile-quantile plots are shown: for the original feature (left column); the feature transformed using the conventional Box-Cox transformation and Raymaekers and Rousseeuw's robust adaptation (middle column); and the feature transformed using the non-robust and robust location- and scale invariant Box-Cox transformations (right column). Samples with observed quantiles below  $-3.0$  or above  $3.0$  are indicated by crosses.

Table E.4: Test statistic  $\tau_{\text{ecn}}$  for empirical central normality at  $\kappa = 0.80$  as a function of Type I error rate for several datasets.

type I error rate	0.50	0.20	0.10	0.05	0.02	0.01	0.001
Box-Cox	0.047	0.073	0.090	0.106	0.126	0.140	0.188
Box-Cox (no outlier)	0.043	0.065	0.079	0.092	0.106	0.116	0.155
Yeo-Johnson	0.041	0.062	0.075	0.088	0.103	0.115	0.154
Yeo-Johnson (no outlier)	0.041	0.061	0.074	0.085	0.099	0.109	0.139
normal distr.	0.039	0.066	0.083	0.097	0.117	0.132	0.174

1. Data sampled from asymmetric generalised normal distributions without outliers.
2. Data sampled from normal distributions without outliers, without any power transformation applied.

Other aspects of the experiment remained the same. Thus, we first drew  $m_d = 10000$  random distributions. For asymmetric generalised normal distributions, each distribution was parametrised with a randomly chosen skewness parameter  $\alpha \sim U(0.01, 0.99)$  and shape parameter  $\beta \sim U(1.00, 5.00)$ . For fully normal distributions, skewness parameter  $\alpha = 0.5$  and shape parameter  $\beta = 2.0$  were fixed. Location and scale parameters were set as  $\mu = 0$  and  $\sigma = 1$ , respectively.  $n = \lceil 10^\gamma \rceil$  values were then randomly drawn, with  $\gamma \sim U(1.47, 3.00)$ , which led to between 30 and 1000 values being drawn to create  $\mathbf{X}_i$ . Residuals were then computed after performing robust location- and scale-invariant transformations with the empirical tapered cosine weighting method for the dataset with asymmetric generalised normal distributions, and without any transformation for the dataset with only normal distributions.

The results are shown in Figure E.14 and Table E.4. These indicate that the test behaves similarly for the different datasets. For low type I error rates, the test statistic proposed in section 3.3 is more conservative than alternatives based on residuals after Box-Cox transformations of asymmetric generalised normally distributed features or on residuals from strictly normally distributed features.

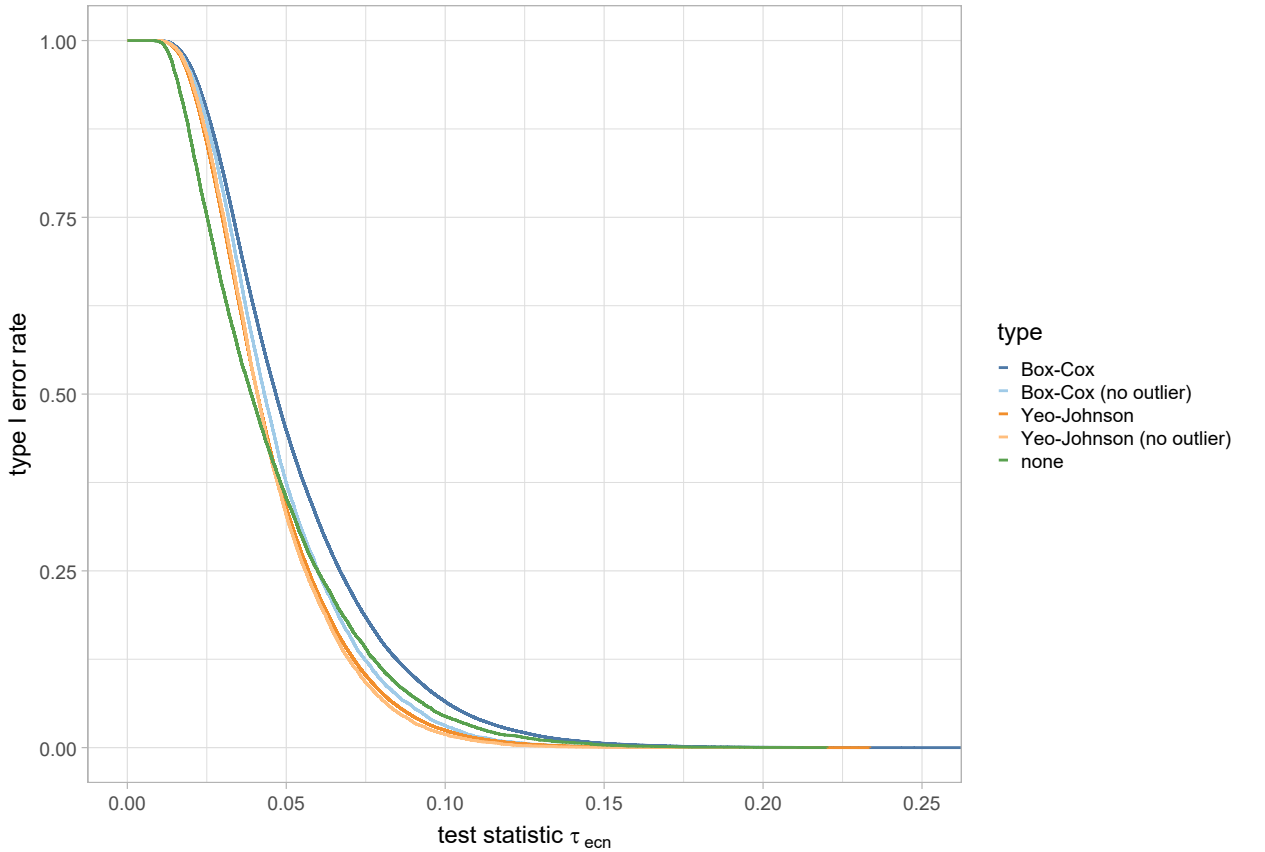


Figure E.14: Type I error rate as function of the test statistic  $\tau_{\text{ecn}}$  for five datasets, with central portion  $\kappa = 0.80$ . The type I error rate is computed from  $m_d = 10000$  randomly sampled features, These are sampled from asymmetric generalized normal distributions, with and without outliers (Box-Cox and Yeo-Johnson), or normal distributions with outliers (none). The test statistic is computed as the average residual of each feature after (Box-Cox and Yeo-Johnson) robust location- and shift-invariant power transformation, or before (none).

Table F.5: Residual errors for features from real-world datasets after Yeo-Johnson transformation to normality. conv.: conventional; norm.: normalisation; rob.: robust

feature	none	conventional	conv. (z-score norm.)	conv. (rob. scaling)	invan
age	16.5	11.5	11.5	11.3	8.
penguin body mass	48.0	32.2	33.3	32.2	26
latitude	328.1	319.0	326.2	324.5	320
fuel efficiency	54.5	55.3	49.0	53.3	44
arterial wall thickness	110.1	30.0	19.3	31.8	12

## Appendix F. Normalisation before transformation

An alternative to location- and scale-invariant transformations is normalising feature distributions prior to conventional transformations. Table F.5 shows residual errors, after transformation to normality, of the five features from real-world datasets presented previously section 4 and Appendix D. In these examples location- and scale-invariant transformations have similar or lower residual errors compared to errors resulting from normalisation prior to transformation.

Example citation, See Lamport (1994).

## References

Leslie Lamport, *TEX: a document preparation system*, Addison Wesley, Massachusetts, 2nd edition, 1994.